A study of high-performance sensing behavior of biosensor based on photonic crystal

Dissertation

Submitted for the Award of the Degree

of

Master of Philosophy

In

Physics

Submitted By

Mohit Kumar

Enrolment No. 553/18

Under the supervision of

Dr. Khem Bahadur Thapa

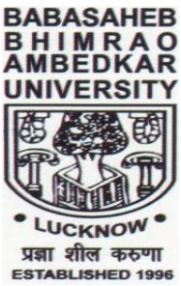

Department of Physics

School of Physical & Decision Science

Babasaheb Bhimrao Ambedkar University (A Central University)
Lucknow – 226025, (U.P.) INDIA

June 2022

CERTIFICATE

This is to certify that the thesis titled **"A study of high-performance sensing behavior of biosensor based on photonic crystal"** submitted by **Mr. Mohit Kumar** is an original research work and has not been previously submitted in part or full for the award of any other degree or diploma to this or any other university.

The M.Phil. dissertation submitted to the Babasaheb Bhimrao Ambedkar University; Lucknow satisfies all the requirements as stipulated in the *Master of Philosophy (M.Phil.)/ Doctor of Philosophy (Ph.D.) regulations amended in 2019* and it is fit for submission and evaluation for the award of the degree of Master of Philosophy of the University.

Date: 28/06/2022

Supervisor

Dr. Khem Bahadur Thapa
Department of Physics
Babasaheb Bhimrao Ambedkar University
Lucknow-226025

Head of the Department

Scanned by CamScanner

DECLARATION

I declare that the thesis entitled **"A study of high-performance sensing behavior of biosensor based on photonic crystal"** has been prepared by me under the supervision of Dr. Khem Bahadur Thapa, Department of Physics, School of Physical and Decision Science, Babasaheb Bhimrao Ambedkar University Lucknow. No part of this thesis has formed the basis for the award of any degree, diploma, or fellowship previously. Further, I declare that the material embodied in the present work is based on original research work and the indebtedness to others has been duly acknowledged at relevant places. This is also declared that the thesis is essentially free from all kinds of plagiarism.

Mohit Kumar

Date: 28/06/2022

(**Mohit Kumar**)

Place: BBAU, Lucknow

Department of Physics,
School of Physical and Decision science,
Babasaheb Bhimrao Ambedkar University,
Vidya Vihar, Raibareli Road
Luckow-226025, U.P., India

Scanned by CamScanner

ACKNOWLEDGMENT

It is my firm belief that any major research work to result in a positive outcome including a worthy thesis requires the culmination of several factors such as a meaningful subject that can motivate a determined researcher to take up the challenge, a learned and sincere guide in the form of friends, relatives, and colleague who selflessly encourage and help the researcher throughout the research. I have the honour and privilege of **Dr. Khem Bahadur Thapa** as an excellent guide. I take this opportunity to place on record my heartfelt and sincere gratitude and deep indebtedness to him without whose guidance this work could not have been meaningfully concluded. I also owe my sincere thanks and a sense of deep gratitude to **Prof. Bal Chandra Yadav**, Head, Department of Physics, School of Physical & Decision Sciences, Babasaheb Bhimrao Ambedkar University, for providing necessary facilities in the department in a very kind behaviour.

I am extremely thankful to my teachers **Prof. Devesh Kumar**, **Dr. Ramesh Chandra, Dr. Anil K. Yadav**, **Dr. Devendra Singh,** and **Dr. Ajeet Kumar Maurya** for their valuable suggestions and encouragement great assets to me during the entire course of study. I owe my deep gratitude to them for their constant motivation and moral support. I feel blessed to have such teachers. Also, I am thankful to staff members at Babasaheb Bhimrao Ambedkar University, especially the **Department of Physics (DOP)**.

I am highly thankful to **Dr. Pawan Singh** for their help and support during the research work and also thankful to our research group members **Dr. Krishan Pal**, **Dr. Asish Kumar**, and **Ms. Abhisikta Bhaduri**, for their support. I would like to acknowledge the contribution of my friends and research scholars, **Mr. Manas Misra, Mr. Mrityunjai Mishra,** and **Mr. Manish Kumar,** to a joyful and healthy environment around my work.

Finally, I would like to pay my highest regard to my grandparents **Late Ram Dulare Saroj** and **Dhanpati Devi**. I owe my indebtedness to my parents **Shri Rajesh Kumar** and **Smt. Leelawati** for their love, support, and sacrifice from the very first day of my journey of life. I am highly thankful to my family for moral support and encouragement.

Last but not least, my final words of thanks will be for Almighty God, for his countless blessings, mercy, and companionship through all turmoil of my life.

Mohit Kumar

(Mohit Kumar)

Scanned by CamScanner

CONTENTS

LIST OF FIGURES

LIST OF TABLE

CHAPTER-1

INTRODUCTION

1.0 Optics

Optics is a branch of physics, studies electromagnetic radiation its interaction with substance, and apparatuses used to gather info due to the interactions. Optics comprises the study of sight i.e. optics is the science of vision. Everybody relies on optics each day viz. wireless mouse, digital camera, and even your Blu-ray discs of your favorite movie and are all technologies empowered by science of the optics [1].

The term optic stands derived from the Greek word οπτικ (optics), which makes both vision and the objective phenomena of light. The vision of the light through the eyes is the one of the five sensors in the human body. The five sensors are used to sense everything around the space namely nose, ear, eyes, skin, and tongue. Hence, in all of them, one most is the eye the sense concerned with this is known as *sight or vision.* Light is the medium to living our sense of sight. The eyes are concerned as a most powerful tool like a signal converter it converts incoming optical (light) signals into electrical signals and also transfers them to the brain after that dealing out the signals causes pictures or images to be formed in our mind. With the use of light, many properties like size and shape of the cosmos and Astro particle-and other properties of a large astral system are studied, by using the property of light reaching us from them after traveling for masses of years through the empty space. The several natural light interactions are occurred around the space that are charms of the rainbow that stretches across the vast sky, the shining sun with the rays of saffron coming out of the sky, the glittering sky with its white clouds, and the exquisite delight of the moon full of enticing stars of a dark night, a celestial spectacle of a total or partial eclipse of the moon and sun. Nature and light structures have been considered since ancient times. Nothing was as obscure or hidden as light. One can gain insight into the nature of light after many centuries of persistent effort [1].

1.1 Historical Overview of Optics

Traditionally, Optics is generally concerned with the natural light of lighting systems that can be traced back to ancient times, with reference to the use of magnifying lenses and

flammable glasses and metal polishing to locate the mirror location the optics subject has dealt. From the modern viewpoint, these are recognized as applications of geometrical optics, although it was not until considered by the ancient Greeks that any kinds of theoretical understanding of these phenomena were endeavored. Most early developments on the subject were based upon the idea that light consists of "rays". The Latin word radius, of which one meaning is a spoke (of a wheel), was used to denote also a ray from the sun so that the divergence of rays in straight lines from a source of light is thus implied. The Greeks were aware of the rectilinear light distribution. They knew that when the light came from the mirror it was equal [1,2].

1.1.1 Development of Geometric Optics/Ray Optics: The first surviving theoretical document was Euclid's Optics (circa 300 BC). Perhaps it is no surprise to the Father of Geometry, that Euclid provided a geometrical account of light, in which he viewed light as the backbone of the eye. His narrative then describes the phenomenon of vision and intangibles. However, the idea that light journeys in a straight line has always been inexplicable. Later, around AD 40, Catoptrica of Alexandria, Hero (or Heron) was showed geometrically that the path of the reflected ray from a plane to an remarkable point is the short travelling possible path that light can take, given the constraint subject to that the ray should touch the plane. In reconsideration, 'the principle of least distance' is called that tolerated a close similarity to a modern clarification. The Hero, however, was not happy that the light travels at different speeds in different material's media and it turns out that the right system can be one of the shortest. Today, this is often described in terms of the length of the visual cue, which is the size of the distance but remains exactly the same as the time taken, which has distance dimensions but it remains directly proportional to the taken of the time. With the end of Greek civilization, the torch of philosophical inquiry rose in the world of Islamic. The mathematical progress of number bases, the development of algebraic and algorithmic methods is well known, if it was not always attributed to Islamic philosophers. One of the earliest contributors to the optics field was Ibn Sahl (c. 940- 1000), in his book "On Burning Mirrors and Lenses" (984) is described the concentration of light in mirrors and bowed lenses. Significantly, it also provides the first detailed structure is nowadays known as Snell's Law of refraction. Another major character was polymath Alhazen (c. 965 - c. 1040). Between 1011 and 1021 Alhazen wrote a seven-

volume optics book entitled Kitab al-Manazir (Book of Optics). During this work, Alhazen performed several experiments on light the rectilinear (in a straight line) propagation of light i.e. called reflection, and refraction. This primary adoption of the Scientific Technique makes Alhazen's work noteworthy work in the more general science history. However, according to optics, his main contribution is often regarded as his detailed explanation of the human eye [1,2].

1.1.2 Wave Optics: Rene Descartes (1596 - 1650) individually based on Snell's Law, termed after Willebrord Snellius (1580 - 1626) and first named by Ibn Sahl, according to the fourth works. Using this concept, he was also able to demonstration that the angular radius of the rainbow from the viewer was 42◦. Although he incorrectly predicted that light would move rapidly with a 'denser' material's medium (i.e., medium with a higher index of refractive) he was still interpreting light as a means of propagating waves, in line with modern theory. Another important concept of optics of wave was given to Dutch physicist Christiaan Huygens (1629 - 1695). Huygens argued his well-known goal that each and every point on the wavefront acts as a source of secondary waves that, sometime later, are combined to provide a new wave. Huygens' system remains a powerful tool for analyzing wave movements, although it can in itself explain why the wavefront travels in a given way rather than slows down again. The definition of this requires the concept of intervention, which we will soon meet. Despite Descartes' acceptance of the interpretation of light wave, Isaac Newton (1642 - 1727) came to reject the idea, preferring the definition of light particles. This theory is well known as the corpuscular light theory. Newton's individual contributions to the optics field were invaluable. Such was Newton's psychological influence on the rise of his power that the corpuscular light theory tended to dominate simply because Newton claimed it. Indeed, it is ironic that when Augustin-Jean Fresnel (1788 - 1827) presented a paper to the French Academy of Sciences in 1818 describing the theory of light waves, Poisson, a member of the jury committee and proponent of corpuscular theory, attempted to challenge Fresnel's work by arguing that this would suggest the appearance of a bright spot in the shadow of an illuminated sphere of light. Moreover, such a bright spot actually exists, now known as the Fresnel bright spot. Although a large number in the development of wave optics, Fresnel's work was partially created by that of Thomas Young (1773 - 1829). Actually, it was Young who gave the first

comprehensive evidence of the nature of light wave at his now-famous double test in 1803. The exhibition of the diffraction phenomenon of light is clearly shown by the double-slit experiment which is incomprehensible in terms of corpuscles (particles). Young's work, was independently discovered by Fresnel, and he is one who added substantially to the diffraction theory as well as being one of the first people to appreciate the importance of the polarization of light. The equation of the reflectance and transmission coefficient ratios of light crossing between different media is also derived from the Fresnel's, now this equation is known by its name [1,2].

1.1.3 Electromagnetism: The wave nature of light had convincingly demonstrated by Young; basic physics needed the electromagnetism theory to be clarified. The theory of electromagnetism builds on the work of several mathematicians and scientists, including Gauss, Coulomb, and Ampere to name a few. One of the main contributors to this field is Michael Faraday (1791 - 1867). Particularly, the law of electromagnetic induction has discovered by Faraday, in which a changing magnetic field is induced a changing electric field. After that James Clerk Maxwell (1831 - 1879), a great physicist, along with his own contributions, combined Faraday's and other laws, into a set of equations that is well known as the Maxwell's Equations. Using these equations, Maxwell was then able to show that a wave equation for self-propagating electromagnetic (EM) waves. Furthermore, by using fundamental universal constants the speed of these waves could be calculated: the permeability and permittivity of free space. This meant that the velocity of EM waves had to be constant. Maxwell actually intended this value and found that this speed of wave (permitting checking error) corresponds to the estimated light speed. Heinrich Hertz (1857 - 1894) successfully established the generation of radio frequency EM waves via the changing electric field of oscillating charge in a dipole antenna. The frequency (SI unit) is called hertz (Hz) in the remembering of his achievement. After this, it was believed that all wave propagation had to happen in some kind of material's medium. The suggested medium for propagation of light was called the 'ether of luminous. In 1887 Michaelson and Morley endeavored experimentally to measure the interaction of the earth and the relative motion of the earth versus the luminous ether by light speed measured at different positions in their orbits through an interferometer. To their amazement, they revealed that the velocity of light was always the same i.e., a very counter-intuitive consequence.

Hendrik Antoon Lorentz (1853 - 1928) modeled this concept by developing the Lorentz transformations and endeavored to explain the phenomenon in terms of 'contraction' of the ether. Though, his transformations also inferred an inexplicable dilation of the temporal space dimension that could not explain. It was completed by Albert Einstein (1879 - 1955) and given that the electromagnetic wave is explained as the light. In 1905, his paper was published on Special Relativity based on the mathematics of the Lorentz transformations and dispensed the idea of 'complete space and time relations', claiming that only relative motion of the light was physically meaningful [3].

1.1.4 Development of Wave Optics: As discussed earlier that the wave theory of light is proposed by Huygens (1629 - 1695), in 1678, which is contemporary of Newton's theory of light. In this theory he is considering that light energy is supposed to be transferred from one place to another by wave form. Huygens was successful in proving elementary laws of light refraction and reflection. He also predicted that the speed of light is faster in rarer medium and slower in denser medium. By considering two types of waves, he also described the phenomena of double refraction. Wave theory was not immediately accepted. The main reason of not acceptance of wave theory is that, for propagation of wave needs medium but the light reached to us from sun without any medium or through vacuum of space that's why it is hard to believe that light is wave.

The interference of light beams was first demonstrated by Thomas Young (1773-1829) in 1803. On the basis of interference of light waves, he also able to explain Newton's ring and the color of thin films. So, after that the wave theory of light is able to achieve a strong support provided by Thomas Young. Further the polarization of light is discovered by Malus (1775 - 1812) in 1808. A satisfactory explanation was given by A. Fresnel (1788-1827) in 1815, he further established the wave theory of light and described the rectilinear propagation of light which has been the principal obstacle in the way of accepting wave theory of light. Also, Fresnel provided an acceptable description of the diffraction phenomena. [2,3].

1.2 Theories of Optics

Here we will briefly discuss four important theories that provide the evolution of optics or the nature of light. The most contributions of the theories are: (a) Corpuscular theory, (b)

Wave theory, (c) Electromagnetic theory and (d) Quantum theory. Now we briefly discuss these theories for evolution of the optics [1,2,3].

1.2.1. Corpuscular Theory: This theory was given by Ancient Greeks and finally suggested by Sir Issac Newton. Perhaps, the corpuscular model is one of the simplest models of light. According to this model, "*a luminous body emits several minutes, rigid, elastic, and massless a stream of particles, named corpuscles, in all directions*." Newton was assuming that particles are very minute to facilitate when two light beams are overlapped, a collision rarely occurs between two particles. In a transparent medium, these particles are able to travel in all directions at a very high speed along a straight line. These corpuscles particles are responsible for our vision by entering our eyes after collision from any stuff followed by a straight-line path and we recognized that material, on the basis of their corpuscles sizes and they yield different colors. These corpuscles particles are attracted by transparent materials and repelled by reflecting surfaces.

There are also have some merits and drawbacks of this theory. (i) **Merits:** (a) this theory describes the straight-line propagation of light; and (b) it is also pronouncing the refraction and reflection of light individually. (ii) **Drawbacks:** (a) the corpuscular theory of light by Newton fails to describe the concurrent phenomenon of partial refraction and reflection on the transparent surface mediums for example glass or water; (b) the optical phenomena like diffraction, interference, polarization, etc corpuscular theory is unsuccessful to describe these all; (c) the consequence of the corpuscular theory of light is the velocity of light is smaller in the rarer medium than in the denser medium and further experimental work it is demonstrated incorrect; and (d) the emitted particle from any light source is constant [1,3].

1.2.2. Wave Theory: A theory is said to be true and complete if it satisfies all observations and experimental phenomena by a smaller number of hypotheses. There are several phenomena that could not be described on the basis of the corpuscular theory of light such as diffraction, interference, and polarization. It's only able to describe the propagation of light through free space and can be made to predict the correct form of laws of reflection. Later was found that the theory is quite unsatisfactory [1,3].

Francesco Grimaldi, about 1665, an Italian physicist, observed diffraction phenomena, when white light is passed through a small aperture and that light is a fluid that exhibits

wave-like motion. Huygens,1678, proposed a theory, in this theory he is assume that light is the wave and this satisfactorily explained diffraction phenomena. Huygens was able to describe the laws of refraction and reflection by the application of the wave theory of light. Danish physicist Erasmus Bartholinus 1669 discovered the phenomena of double refraction which is also explained by Huygens. The people around the newton had more belief in the corpuscular theory of light than Newton himself no one believed in Huygens's theory until 1801 when the famous interference experiment had been done by Thomas young which could be described interference on the basis of wave theory [1,2,3].

1.2.2.1. Huygens Wave Theory: This theory can permit us to determine the shape of a wavefront at any time if the earlier time of shape of the wavefront is known as the Huygens wave theory which is mainly based on a geometric construction in the shape of a wavefront. A wavefront can be defined as the locus of the points, which are in the same phase [1].

Several postulates have been given by Huygens wave theory are given, which is as follows :–

1. A light source emits light in the form of waves.
2. The nature of light waves is longitudinal in nature like sound waves.
3. The speed of light waves is a constant in a homogeneous medium.
4. Different colors of light have different wavelengths of waves.
5. The sensation of vision or sight is due to the light waves entering our eyes.
6. A aluminiferous ether is present in a vacuum which is responsible for the motion of light waves in a vacuum.

This theory has several merits and demerits. (i) **Merits:** (a) there are a number of phenomena such as refraction, reflection, diffraction, and interference explained by the wave theory of light; (b) the wave theory of light gives a satisfactory explanation of the phenomenon of partial refraction and reflection of light; and (c) the light wave travels faster in a rarer medium and slower in a denser medium according to the wave theory of light, which is correct. (ii) **Demerits:** (a) it is assumed that there is hypothetical ether medium present for propagation of light wave according to the wave theory of light but it is experimentally proved that there is no ether or drag; (b) the wave theory of light is unable

to describe rectilinear propagation of light; (c) the polarization of light and Compton effect could not be described by the wave theory of light; (d) The bending of waves through any obstacle also could not explained by wave theory of light; and (e) further, it is experimentally proved that the light waves are transverse waves but according to wave theory of light it is assumed that light waves are longitudinal in nature which is proved incorrect [1,3].

In general, the Huygens' principle can be stated as follows:

- Every point of a wavefront can act as source of a secondary wave which can emit light in all possible direction.
- Only those secondary waves taken to be effective which progressing in forward direction.
- The locus or tangential surface to all these secondary waves at any instant gives a new wavefront at that given instant.

According to Huygen's geometrical construction, it is likely to determine the nature and conceivable to regulate the wavefront's nature and position at a later instant if the nature and position of the wavefront at the assumed instant are known. The construction of spherical wavefront is given as; suppose, the cross-section AB of spherical wavefront at any instant, which is emitted from a point source. This can be termed as primary wavefront. Now on the wavefront AB considering three points P, Q, R as shown in the Fig.1.1. Thus, every point acts as a source of secondary waves and can produce secondary wavelets according to Huygens' principle. In any medium, the speed of light is 'c' then at any time 't' every wave will travel a distance 'c*t' in onward direction and the secondary waves that moving in reverse direction does not exist. The P, Q, R are the centers of circle with radius 'ct'. These all circles represent a secondary wavefront. The new position of the wavefront after time 't' represents common tangential surface A'B' drawn to these secondary wavefronts [1].

Similarly, the construction of plane wavefront is also given as; Suppose, the cross-section AB of plane wavefront at any instant, which is emitted from a point source. This can be termed as primary wavefront. Now on the wavefront AB considering three points P, Q, R as shown in the Fig. 1.2.

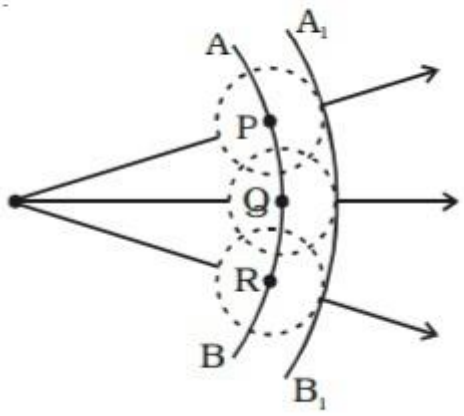

Figure: 1.1: Construction of spherical wavefront [1].

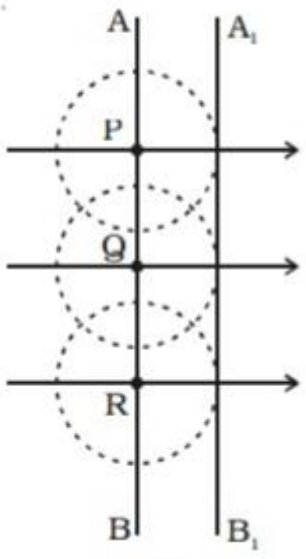

Figure: 1.2: Construction of Plane wavefront [1].

Thus, every point acts as a source of secondary waves and can produce secondary wavelets according to Huygens' principle. In any medium, the speed of light is 'c' then at any time 't' every wave will travel a distance 'ct' in onward direction and the secondary waves that moving in reverse direction does not exist. The P, Q, R are the centers of circle with radius

‘c*t’. These all circles represent a secondary wavefront. The new position of the plane wavefront after time ‘t’ represents common tangential surface A'B' drawn to these secondary wavefronts [1].

1.2.3 Electromagnetic Theory: The electricity and magnetism equations had successfully developed by Maxwell 1862 ingeniously and the equations of these summarily combined and give the famous equation of electromagnetic theory. He also introduced that the velocity of electromagnetic waves (EMW) is the same as the velocity of light and hence he concluded that the light wave itself is electromagnetic waves initially; for the propagation of electromagnetic waves in space has been assumed ether medium i.e., the existence of ether medium. However, if light waves which are very high frequency are to propagate and at the same time allow a free passage to heavenly bodies, then the ether has to be rigid as well as pliable. It became impossible to visualize the hypothetical solid which could an easily compressed or expanded, could permit resistance-free passes of heavenly bodies through it, and yet be elastic to twisting or bending stresses in order to allow propagation of waves. Ultimately, in 1887 Michelson and Morley proved conclusively that there was no ether surrounding the earth or elsewhere [1,2,3].

1.2.4 Quantum Theory: In 1900 Max Planck gives the first real breakthrough by introducing the concept of quantum of energy or quanta. He postulated that the exchange of energy between radiation and its surrounding takes place in the quantized form or discrete form. Only after postulating this, he is able to successful to explain the phenomena of blackbody radiation and reproduce through the experimental results. Max Planck argued that if v is the frequency of electromagnetic wave (EMW) then the energy exchange between matter and electromagnetic wave only occurs in integer multiples of hv. A powerful consolidation of Planck’s quantum concept is provided by Einstein in 1905. Planck and Einstein recognized the idea of quantization of electromagnetic waves. It is also useful for trying to understand of photoelectric effect and be effective for light too. Planck’s approached that light is itself made up of isolated bits of energy are termed as photon or quanta each have energy hv where v is the frequency of light. A most conclusive confirmation is concluded by Compton in 1923, he discovered the corpuscular nature of light. Compton made an important invention that provided the most decisive validation for the corpuscular aspect of light. By the confirmation of particle nature of X-ray photon with

momentum h*v*/*c*; *v* is the frequency of the X-rays via scattering X- rays with electrons. Further confirmation for the quantum theory is obtained when the Compton Effect is discovered in 1923. Compton found that the monochromatic x-rays fell upon the matter the scattered rays contained not only the original rays but also x-rays of wavelengths longer than the originals. The quantum theory explains successfully the interaction of radiation with matter it cannot account for the phenomena of polarization, interference, and diffraction. The contradictory aspects are reconciled by the postulating dual nature of radiation. Accordingly, radiation is viewed as having both particles as well as wave nature [1,2,3].

1.3 Optical Density

In optics, when the light beam is passed through one medium to another then the ratio of the light in two media is called the optical density or refractive index of materials. In other words, it is the ability of a material to pass the light [1,2,3].

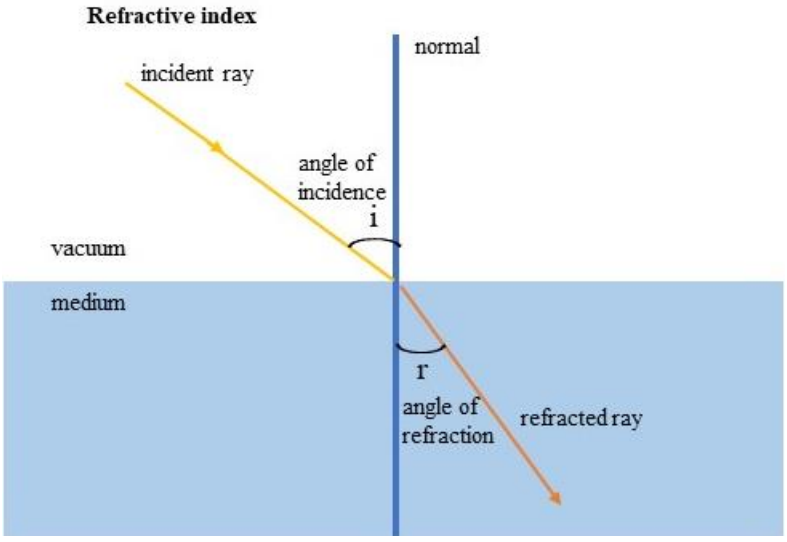

Figure: 1.3 Refraction property of optical wave in two different media [1,2,3].

1.3.1. Refractive Index of the materials: This is the property of the medium since it depends on the permittivity and permeability of the medium. The refractive index (RI) or optical density is the ratio of the velocities of light in vacuum and medium. If the angle of

the incident ray is <i, and the angle of the refractive angle is <r (Fig. 1.3); then the refractive index (n) is defined as;

$$n=\sin(<i)/\sin(<r) \quad (1.1)$$

The optical density is also equal to the ratio of the speed of light (c) of a given wavelength in empty space to its speed v in a medium,

$$n=c/v \quad (1.2)$$

The optical density is used to differentiate the properties of the material medium that deduced the optical wave propagation through the medium [1].

There are several media based on the different optical densities. These media are:

- **Linear medium**: A differential equation can accurately modeled propagation of wave in any linear medium so the consequence of this we may construct linear superposition of the solutions. Only the linear displacement is considered in any linear mediums that is why we called linear medium.
- **Isotropic medium**: If the properties of materials are same in all directions, then it is called an isotropic medium. In isotropic medium the optical density does not depend on the direction of the propagation or orientation of polarization. On the other hand, materials with property of directional dependence are known as anisotropic
- **Homogeneous medium**: Materials with properties having same everywhere is called a homogeneous medium. These materials do not depend on the spatial positions. On the other hand, Materials with properties having different everywhere, means dependent on spatial position is called inhomogeneous [1,2,3].

1.3.2. Relation Between the Refractive Index and Relative Permittivity of a Medium: The velocity of propagation v of the light in a medium of permittivity ε and permeability μ is simply given by Maxwell's equations [1,2,3]

$$v=\sqrt{\frac{1}{\epsilon\mu}} \quad (1.3)$$

and the velocity of light in vacuum is

$$c = \sqrt{\frac{1}{\epsilon_o \mu_o}} \tag{1.4}$$

for the case of medium $\varepsilon = \epsilon_r \epsilon_o$ and $\mu = \mu_r \mu_o$.

So, the equation (1.3) can be rearranged;

$$v = \sqrt{\frac{1}{\epsilon_r \epsilon_o \mu_r \mu_o}} \tag{1.5}$$

so, the refractive index of the medium is given as;

$$n = \frac{c}{v} = \sqrt{\epsilon_r \, \mu_r} \tag{1.6}$$

For the non-magnetic medium, the relative permeability is one i.e. μ_r=1, therefore the refractive for dielectric medium is;

$$n = \sqrt{\epsilon_r} \tag{1.7}$$

$$n^2 = \epsilon_r \tag{1.8}$$

1.3.3. Malus's Law: France's engineer Malus, 1808, had found that when an un-polarized light beam is propagated in any direction and incident on polarizer then the transverse electric vector associated with it oscillates. Malus proposed that if the amplitude of the electric vector is E_o then the emerging electric vector from the polaroid is $E_o \cos\theta$ and thus the intensity of the beam is

$$I = I_o \cos^2\theta \tag{1.9}$$

where I_o is the intensity of the beam [1,2,3].

1.3.4. Law of Polarization or Brewster's Law: Brewster's, 1811, according to this law if the sum of incident angle and refraction angle is $\frac{\pi}{2}$ then there is no reflected beam. At certain angle when an unpolarized beam of light is an incident such that

$$i + r = \frac{\pi}{2} \tag{1.10}$$

then the reflected light will be polarized while vector E is perpendicular to the incidence plane and parallel component of the E vector will not be reflected. This particular incidence angle is called the polarizing angle or Brewster angle and denoted by i_p.

$$i_p = tan^{-1}\frac{n_2}{n_1} \tag{1.11}$$

where n_1 and n_2 are the refractive index of the mediums [1,2,3,4].

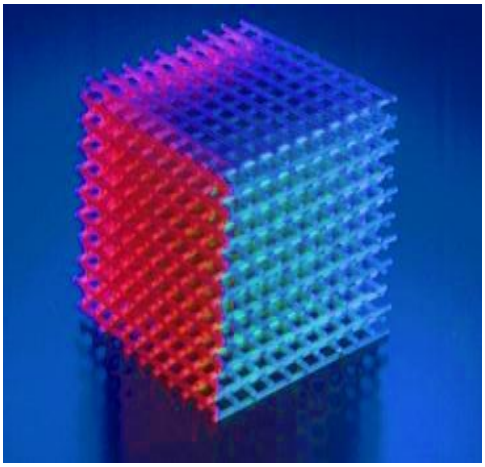

Figure: 1.4: Three-dimensional Photonic crystal in the Yablonvite structure [6].

1.4 Photonic Crystals

A solid composed of atoms arranged in periodic pattern in three dimensions is called the crystal. The pattern of the molecules or atoms are arranged in the repetitive pattern in space is termed the crystal lattice. It is analogous that electrons are felt a periodic potential in crystals and propagate through this potential and also, they form the geometry of the crystal as well as the conductivity of the crystal. In general, a periodic dielectric structure can interact resonantly with radiation with wavelength eqiual to the periodicity length of the dielectric lattice. Photonic crystals can affect the properties of photons in much the similar way that conductor and ordinary semiconductors crystals affect the properties of electrons, like a semiconductor has an electric bandgap where the electron cannot propagate with less energy than the bandgap similarly the Photonic crystal materials have periodically modified refractive index and exhibit photonic bandgap. So, the electromagnetic wave in which cannot propagate that is called forbidden. The Bloch Floquet theorem is likewise governed for the study of photonic crystals, and analogous to electronic dopants in

electronic materials here also intentionally introduced defects in the photonic crystals that produce the localized electromagnetic states: point-like cavities and waveguides. Thus, the crystals may form a type of perfect "insulator," this insulator can be confined localized electromagnetic states or light lossless around sharp bends, in low-index media, and within wavelength-scale cavities, including other novel possibilities for controlling of the electromagnetic phenomena (Fig. 1.4) [3,4,5].

1.4.1. History of Photonic Crystals: English physicist Lord Rayleigh 1887, had first invented propagation of the electromagnetic wave in a periodic media with periodic multilayer dielectric stacks, showing a photonic bandgap in one dimensional. In the issues of "Philosophical Magazine," the idea of a one-dimensional photonic crystal has been derived itself very earlier in the partly titled paper, "The propagation of wave through a medium Endowed with a periodic structure". In terms of modulation period, 'a' Rayleigh comprises a modern observing formula for the boundaries of the forbidden gap and of the periodic density modulation relative strength $\frac{\rho}{\rho_o}$ that is related with the incident wavelength;

$$\frac{\lambda^2}{4a^2} - 1 = \pm\frac{\rho_1}{2\rho_o} \tag{1.12}$$

In an addendum, Rayleigh was written about that application of these ideas to light incident on a layered silver structure produced by interference exposure of a photographic medium. In addition, in 1888, Rayleigh stated that the wave propagation in an infinite layered madia having the harmonic periodic waves. Due to this periodicity of the media with harmonic waves, the ultimately total reflection occurred that provided the agreement of varied sufficient value close between the wavelength of the periodic structure and half-wavelength of the wave. Rayleigh had already recognized the definite magnitude of the forbidden or stop-band on the basis of this prediction and also understood well that even a microscopic periodic variation in the structure would produce a band gap, and that it would make a "total reflection mirror". That a stop band gap could arise, even from microscopic modulation, is peculiar to the one-dimensional situation. It is well-defined that Rayleigh had stop band gap in the "laminated" one-dimensional structures.

We know the study of photonic crystal was done in 1887, but the term of the photonic crystal was used after 100 years by E. Yablonovitch and S. John in the 1987 when S. John and E.Yablonovitch published two papers in PRL in same volume [6,7]. These two millstone papers were acted as advancements in the way of photonic crystals. In 1987, the American Physical Society was recognized as one of the landmark developments in the field of optical physics after that the early history can be well predictable in the form of a story, and further exponentially began to grow the number of research papers about photonic crystals. Because of the difficulty of inventing these structures at optical scales, preliminary studies were conducted where photonic crystals could be fabricated on a more accessible centimeter-scale, either theoretically or under microwave control. In short, electromagnetic fields are solutions to Maxwell's equations, which have no natural length scale. Therefore, the resolution of a centimeter to the nanometer-scale structure at optical frequencies is similar to a centimeter-scale structure in a microwave [1,2,3,4,5].

In 1991, Yablonovite have been demonstrated the first 3DPC bandgap in the microwave regime. In a transparent material, Yablonovite was able to produce structure by drilling an array of holes, however, an inverse diamond structure formed the holes of each layer. At this time recognized as Yablonovite structure [4]. T. Krauss et al. [11] demonstrated a 2DPC at visual wavelength. This demonstration opened a new window on the way to manufacture semiconductor material for the photonic crystals by borrowing approaches from the semiconductor material.

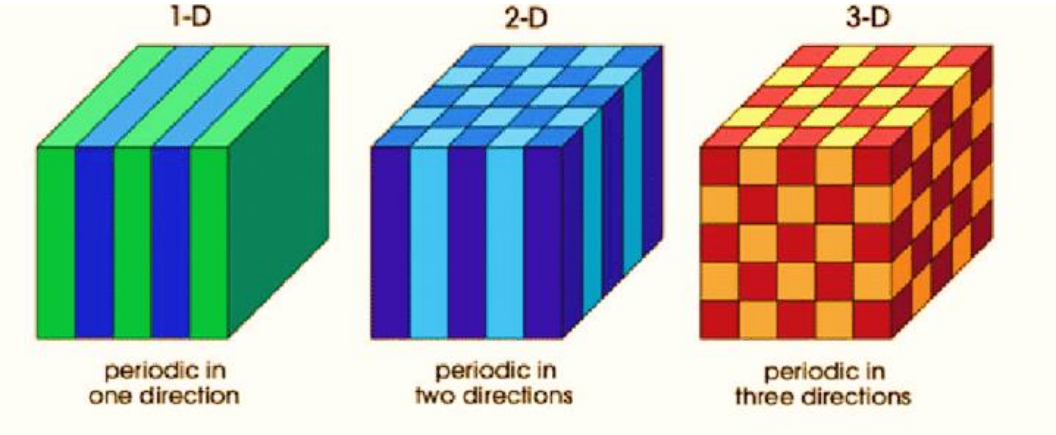

Figure 1.5: Types of photonic crystals: 1-D, 2-D and 3-D photonic crystals [4]

1.4.2. Types of Photonic Crystals: According to their definition of the photonic crystals, if the wavelength of radiation is comparable to the periodicity length of the dielectric lattice, then the photonic crystals can interact resonantly with radiation. On the variation of refractive index with dimension photonic crystal has been divided in three types. There are one dimensional (1DPC), two dimensional (2DPC) and three dimensional (3DPC). If the variation of refractive index is in one direction, then this is called one-dimensional photonic crystal [4].

We now briefly described the 1-D, 2-D and 3-D photonic crystals: (i) **1DPC:** The dielectric constant stands periodically modulated in one dimension. The optical properties are known it is a dielectric multilayer. These are employed as anti-reflection coating and high reflection mirrors. (ii) **2DPC**: The dielectric constant is periodically modulated in two dimensions. Its intersection of air or dielectric rod axes with perpendicular plane from 2D lattice. Therefore, how the 2DPC formed. (iii) **3DPC:** The dielectric constant is periodically modulated in three dimensions. Lattice is defined by 3 primitive vectors. If we design a property where a range of frequency cannot propagate because there is no electromagnetic eigenmode exists. This kind of frequency is called a photonic bandgap. Subsequently there correspond to band gaps of electronic eigenstate in regular crystals. Likewise, if we are introduced a disorder into the ordinary dielectric periodic structure of the photonic crystal, then we are obtained a band gap mode, whose eigen function is strongly localized around the disorder. Such mode is called localized mode.

The periodicity of the refractive index in the PCs plays important role in the formation of the stop bonds. Hence, **t**he refractive index (RI) or optical density is the critical parameter for controlling the propagation of the electromagnetic wave in an optical material. In general, a very special kind of property has been shown by periodic multilayered material because of the periodicity of the optical density of the materials for the control of the propagation of electromagnetic wave. The multi-layered periodic structure shows obstruction of finite range of frequencies in transmission, known as photonic band gaps (PBGs) [8,9,10]. This kind of multilayered periodic structures is called as photonic crystals [4,11,12]. The PCs are several numbers of different applications due to existence of the PBGs such as optical sensors, biosensors, switches, reflectors, optical filters, etc. [8,13].

1.5 Sensor and Optical Sensor: A sensor is a device that receives and responds to definite input from the physical system. The specific input can be electron, light, heat, and motion of molecules, moisture, pressure, and any one of the parameters that change the physical phenomena of the system. Based on the physical changes, the sensors are divided into various types of sensors such as temperature sensor, pressure sensor, optical sensor, biochemical sensor, microphone sensor, digital sensor, a mechanical sensor, etc. Of these sensors, the most durability has optical sensors have high efficiency and high accuracy.

Generally, an optical sensor is an analytical device that converts the number of analytes into a detectable signal. The evanescent field wave phenomenon is used as an optical sensor to monitor changes in the optical density which occurs within a few hundred nanometers of the sensor surface. Similarly, the change in biological as well as chemical reactions is noticed by a tool or device, which is based on the creation of signals in responses to applied data or values and is generally termed a biosensor. This type of biosensor has potential applications in the biological effects such as detection and disease monitoring, detection of contamination, and disease markers in bodily fluids. These optical sensors are the most desirable due to their ultra-compact size with high accuracy and, high efficiency, which are highly suitable for photonic integrated circuits and various sensing applications. The research on optical sensors that are based on photonic crystals is going on due to the tunable bandgap of the photonic crystals [13-15,17-23].

1.5.1 Biosensor: The change in biological as well as chemical reactions is noticed by a tool or device, which is based on the creation of signals in responses to applied data or values and is generally termed a biosensor. This type of biosensor has possible applications in the biological effects such as detection and disease monitoring, detection of contamination, and disease markers in bodily fluids [24,25]. Due to the enhancement of field in photonic crystal there is also have significance in bio-photonics for the biosensing application, sensitivity towards biomaterials [13-15]. Essentially, a device that receives and responds to definite input from the physical system is termed a sensor. [16]. The specific input can be electron, light, heat, and motion of molecules, moisture, pressure, and any one of the parameters that change the physical phenomena of the system. Based on the physical changes, the sensors are divided into various types of sensors such as temperature sensor, pressure sensor, optical sensor, biochemical sensor, microphone sensor, digital sensor,

mechanical sensor, etc. [17-23]. Of these sensors, the most durability has optical sensors have high efficiency and high accuracy. The evanescent field wave phenomenon is used as an optical sensor to monitor changes in the optical density, which occurs within a few hundred nanometers of the sensor surface [24]. These optical sensors are the most desirable due to their ultra-compact size with high accuracy and, high efficiency, which are highly suitable for photonic integrated circuits and various sensing applications. The research on optical sensors that are based on photonic crystals is going on due to the tunable bandgap of the photonic crystals [19]. Similarly, the change in biological as well as chemical reactions is noticed by a tool or device, which is based on the creation of signals in responses to applied data or values and is generally termed a biosensor. This type of biosensor has possible applications in the biological effects such as detection and disease monitoring, detection of contamination, and disease markers in bodily fluids [24,25].

1.6 Surface Plasmon Resonance (SPR)

The collective oscillation of conduction band electrons that are in resonance with the oscillating electric field of incident light is called Surface plasmon resonance (SPR), which through non-radiative excitation will produce energetic plasmonic electrons. In most popular biosensors they used the property of metal of surface plasmon resonance (SPR). The SPR property of the various metals is used in most of the widespread biosensors. The surface electrons on metal are get stimulated by when light wave is incident at a particular angle, consequently electrons of metal surface become stimulated by incident photons after that propagate on the metal surface. If both frequency as well as momentum have same in photons excitation then the surface plasmon polariton are produced. Therefore, the surface plasmon polariton wave are used in SPR biosensor to detect the change in the coupling effects of biomolecules and surface of sensing materials and it is also kind of optical sensor. In the surface plasmon polariton of metal-dielectric periodic materials, the vertically confined refracting electromagnetic wave is called a surface plasmon polariton and these propagating waves are used only as a sensor at the interface between the metal and the dielectric layer (sensing material). [21,24,25]. The trigger surface plasmon resonance on the metal surface depends on the refractive index (RI) of the material, which is embedded with the metal surface by considering the constant wavelength and angle of incidence of the light. Therefore, a small change in the optical density of the sensing media drives the

expression of surface plasmon resonance to detect analytes. In the surface plasmon resonance assay, analytes are computed by monitoring the intensity of the scattered field or by tracking changes in the resonance angle; Which makes real-time and label-free exposure technology useful in bio-sensing applications. To date, the variety of SPR biosensors has advanced technically to determine clinically suitable biomarkers. Several nanomaterials are also used to improve the detection responses of surface plasmon resonance biosensors. Surface plasma resonance is theoretically an important component of real-world systems such as biological analytical devices [26-30], optical bistability devices [31], and THz filters [32]. In addition, SPR is highly regarded for acquiring SPR sensor devices that offer unique benefits such as real-time analysis and high reliability and high sensitivity [33].

1.6.1 Long Range Surface Plasmon Resonance (LRSPR): A long-range surface plasmon resonance (LRSPR) is a special electromagnetic field mode excited by adding a low refractive index dielectric buffer layer between the substrate and the metal layer on the basis of conventional SPR. Due to the lower loss, longer propagation distance and deeper penetration depth of surface plasmon polaritons in LRSPR sensor, LRSPR sensor has better sensitivity, full width at half maximum of resonance dip and refractive index resolution than conventional SPR sensor. Therefore, LRSPR sensor is more suitable for the detection of biological macromolecules and even cell structure.

1.6.2 LRSPR based Biosensor: LRSPR sensor is used the detection of biological macromolecules and even cell structure because it has the lower loss, longer propagation distance and deeper penetration depth of surface plasmon polaritons. In the LRSPR sensing medium, variation in the concentration of biomolecules yields a local change in the refractive index in contact of metal surface. The modified optical density leads to a variable diffusion constant of the SPP and can alternatively be measured by the attenuated total reflection technique. Here, the TM polarized surface plasmon wave is excited by metal thin film, however the long-range surface plasmon resonance (LRSPR) based prism with metal-dielectric interfaces is embedded in the intermediate layers [34]. Since, many representative studies have been done based on the LRSPR. Matsubara et al. [35] described to achieve high analysis accuracy for the application of long-range geometry SPR sensor. However, the demand and development of high durability with maximum sensitivity, better

detection accuracy (DA) and more optimized LRSPR based sensors are growing in this field of interest from last few couple of years. In the conventional LRSPR based sensors, Gold (Au) is implemented as the metal constituent, but it is not able to process oxidation, additionally, it also does not react with utmost chemicals. Besides, these Au-based sensors show some inefficient sensing responses and DA i.e., they are small values [36,37]. In order to achieve enhanced sensitivity of a biosensor device, the desirable parameters are the better DA and the more stability than the conventional biosensors. Here, we have proposed different kinds of metal-MoS_2 and metal-Perovskite LRSPR biosensors. The sensing behaviors of the proposed biosensors have been studied. Moreover, we have also compared the optical responses of metal-graphene, metal-MoS_2 and metal-Perovskite LRSPR biosensors. The Perovskite ($CH_3NH_3PbBr_3$) material has unique feature of its outstanding photoelectric, thermal and electrical properties. So, Perovskite materials are widely used in solar cells, photoluminescence converters, microwire lasers, and other fields. Consequently, $CH_3NH_3PbBr_3$ Perovskite has used in the field of optical LRSPR sensors. Wu et al. investigated the sensitivity of the LRSPR biosensor with cytop/Al/graphene configuration and found that the sensitivity is enhanced greatly by the introduction of the graphene layer in the LRSPR biosensor configuration [38].

1.7 Objective of Dissertation

The objective of the dissertation was to study of high-performance sensing behavior of biosensor based on photonic crystals. In this sequence of the study, surface plasmon resonance (SPR) and long-range surface plasmon resonance (LRSPR) based biosensors of different Kretschmann configurations investigate theoretically. These considered Kretschmann configurations compare with standard or conventional SPR and LRSPR cytop/Al/graphene configuration biosensor [55,59,60]. We use transfer matrix method for TM mode to calculate the optical properties of considered configurations for desired application of biosensors. The reflectance of the considered configurations for designed biosensors investigates sensitivity, full width at half maximum and detection accuracy with variation of optical parameters of the structure as well as the parameters of the materials. On the basis of the calculation of sensitivity, detection accuracy, and efficiency, we propose a high-performance sensing behavior of biosensor based on photonic crystals having SPR and LSPR properties.

CHAPTER-2

THEORY AND METHODOLOGY

In the optics, the interaction of electromagnetic waves (EMWs) with any material or medium depends on the refractive index or dielectric function or optical density of the medium, which gives the degree of propagation of EMW in materials. The interaction of the electromagnetic wave with the material or medium also depends on the surface and interacting material type. The refractive index (n) of the medium is associated to the electric permittivity (ε) and the magnetic permeability (μ) of the material. The refractive index is the square root of the product of electric permittivity (ε) to magnetic permeability (μ) which is given as;

$$n = \pm\sqrt{\varepsilon\mu} \tag{2.1}$$

Its wave propagation vector, gives the directional propagation of EMWs through the material is given by,

$$\vec{k} = \frac{n\omega}{c}\hat{k} \tag{2.2}$$

The interaction of EMW with any material exhibits reflection and refraction of the incident wave at the material interface, and these effects follow the Snell's law as;

$$n_1 sin\theta_1 = n_2 sin\theta_2 \tag{2.3}$$

where n_1, n_2 are refractive indices of the first, second medium, respectively, and θ_1, θ_2 are incident angle, refraction angle of EMW at the material interfaces, respectively. The refractive index is also can be defined as [3,4];

$$n = \frac{c}{v} \tag{2.4}$$

2.0 Maxwell's Equations

Maxwell's equations those govern, including the light propagation in photonic crystal and all macroscopic electromagnetism. In differential form, these are in SI units-

$$\nabla \cdot D = \rho \tag{2.5}$$

$$\nabla \cdot B = 0 \tag{2.6}$$

$$\nabla \times E = -\partial B / \partial t \tag{2.7}$$

$$\nabla \times H = j + \partial D / \partial t \tag{2.8}$$

where ρ and j represent the charge and current densities respectively; D, B, E, and H represent the electric displacement vector, magnetic induction, electric field, and magnetic field respectively.

In the entire first equation is Gauss's law, which states that the electric displacement vector D divergence is the free charge density ρ. In other words, D is the source or sink of the free charge. The relation between electric displacement vector D, electric field E, and electrical polarization P of a material medium is related to such as;

$$D = \varepsilon_o E + P \tag{2.9}$$

where ε_o is known as the permittivity of free space which is constant for free space. The second one is the Maxwell's law which stating that the magnetic field B divergence is zero, that means there is no magnetic monopoles so, B has no sources or sinks. Eventually, like a loop every magnetic field line is a join up itself, a closed curve. Third equation is electromagnetic induction, which is given by Faraday, which states that a non-conservative electric field is generated by changing magnetic field. The scalar potential Φ and a conservative vector field F is related to such as;

$$F = -\nabla \Phi \tag{2.10}$$

The curl of this, $-\nabla \times \nabla \Phi$ will be identically zero because the curl of the divergence is always zero vector identity rule. So consequently, $\nabla \cdot \nabla \times E$ is also becoming zero, in the sense that there is no source or sink of the induced electric field and that the field lines are closed curve, all sum up in loops. The last equation is the modified Ampere's Law where the displacement current density is added, when Maxwell realized that the charge conservation must be required. Ampere's law relates the field vector H curl to the free current density. The magnetic field H, magnetic induction B and the magnetization M of a material medium is related by;

$$H = \frac{1}{\mu_o} B - M \tag{2.11}$$

where μ_o is the permeability of free space.

For linear, homogeneous and isotropic mediums the constitutive relations can be written as the equations: D=εE , j=σE and B=μH, where ε, σ and μ represent the permittivity, conductivity and permeability of the medium respectively [3,4].

2.1 Plane Wave in Dielectric Medium

Consider a non-charged current free dielectric medium having ρ=0 and J=0. Further if we use the first and third equations of Maxwell's equations for dielectric medium and the constitutive relations give as;

$$\frac{\partial E_x}{\partial x} + \frac{\partial E_y}{\partial y} + \frac{\partial E_z}{\partial z} = 0 \tag{2.12}$$

$$\frac{\partial H_x}{\partial x} + \frac{\partial H_y}{\partial y} + \frac{\partial H_z}{\partial z} = 0 \tag{2.13}$$

$$\left.\begin{aligned} \frac{\partial E_z}{\partial y} - \frac{\partial E_y}{\partial z} &= -\mu\frac{\partial H_x}{\partial t} \\ \frac{\partial E_x}{\partial z} - \frac{\partial E_z}{\partial x} &= -\mu\frac{\partial H_y}{\partial t} \\ \frac{\partial E_y}{\partial x} - \frac{\partial E_x}{\partial y} &= -\mu\frac{\partial H_z}{\partial t} \end{aligned}\right] \tag{2.14}$$

and

$$\left.\begin{aligned} \frac{\partial H_z}{\partial y} - \frac{\partial H_y}{\partial z} &= \varepsilon\frac{\partial E_x}{\partial t} \\ \frac{\partial H_x}{\partial z} - \frac{\partial H_z}{\partial x} &= \varepsilon\frac{\partial E_y}{\partial t} \\ \frac{\partial H_y}{\partial x} - \frac{\partial H_x}{\partial y} &= \varepsilon\frac{\partial E_z}{\partial t} \end{aligned}\right] \tag{2.15}$$

Now, we will study the properties of plane waves by Maxwell's equations. The plane wave propagation for the electric field and the magnetic field in the direction of k can be written as;

$$E = E_o \exp[i(kz-\omega t)] \tag{2.16}$$

$$H = H_o \exp[i(kz-\omega t)] \tag{2.17}$$

where E_o and H_o might be a general complex quantity and these vectors are independent from space and time.

Subsequently E and H are independent of x and y then the equations 2.12 and 2.13 give

$$\frac{\partial E_z}{\partial z} = 0 \tag{2.18}$$

$$\frac{\partial H_z}{\partial z} = 0 \tag{2.19}$$

Since our interest in solution of the plane wave equation given by equation (2.14) and (2.15), we must have the fields with $E_z = 0$ and $H_z = 0$. Therefore, the waves are transverse type because the longitudinal components are vanishing. Now, we can choose the E along the x-axis without any loss of generality, thus we can assume $E_y = 0$.

Using equations, we simplify to the equations with above conditions and the equations become;

$$0 = i\omega\mu H_{ox} \tag{2.20}$$

$$ik E_{oy} = i\omega\mu H_{oy} \tag{2.21}$$

and $$-ik H_{oy} = -i\omega\varepsilon E_{ox} \tag{2.22}$$

$$ik H_{ox} = 0 \tag{2.23}$$

where $$E_0 = x\hat{} E_{0\,x} + y\hat{} E_{0\,y} + z\hat{} E_{0\,z} \tag{2.24}$$

$$H_0 = x\hat{} H_{0\,x} + y\hat{} H_{0\,y} + z\hat{} H_{0\,z} \tag{2.25}$$

i.e., E_{ox}, E_{oy} and E_{oz} are the x, y, and z components of E_o etc.

The equations give $H_{ox} = 0$ and $\frac{H_{0y}}{E_{0x}} = \frac{k}{\omega\mu} = \frac{\omega\varepsilon}{k}$. Consequently, the plane wave as denoted by equation and indeed satisfy Maxwell's equation with

$$k^2 = \omega^2\varepsilon\mu \tag{2.26}$$

which is dispersion relation in isotropic medium. We obtain the propagation constant $k=\omega\sqrt{\varepsilon\mu}$. If we define refractive index (n) = $\sqrt{\frac{\varepsilon\mu}{\varepsilon_o\mu_o}}$, where $\mu_o = 4\pi \times 10^{-7} N\text{-}sec^2C^2$ $\varepsilon_o = 8.85\times 10^{-12} C^2/\text{N-}m^2$.

Suppose if the x-axis is the direction of electric field vector, so then the y-axis is the direction of magnetic field vector. The electromagnetic waves are transverse in nature then the electric field and magnetic field can be composed as;

$$E = \hat{x}\, E_o \exp[i(kz-\omega t)] \quad (2.27)$$

$$H = \hat{y} H_o \exp[i(kz-\omega t)] \quad (2.28)$$

Thus $c=\frac{1}{\sqrt{8.85\times 10^{-12}\times 4\pi \times 10^{-7}}} = 2.99794 \times 10^8$ m/sec and the c denote the velocity of propagation of electromagnetic waves (EMW) in free space [3,4].

2.2 Transfer Matrix Method (TMM) for Periodic Media

The transfer matrix method (TMM) is derived on the solutions of Maxwell's equations in the isotropic or anisotropic medium and such method connects the electric field or magnetic field on both sides of a layer. Depending on the type of material, the coupling of the electric field and magnetic field are varied, which forms the characteristics matrix having 2x2 matrix forms using boundary conditions. The calculation of the optical properties of dielectric periodic materials is analogous to the calculation of the electronic properties of periodic atomic potentials in the materials. The eigen values of the wave function of periodic atomic potentials can be solved by the Schrödinger's equation. Similarly, eigen values of dielectric functions are also solved for the photonic crystals by Maxwell's equations and eigen values can be obtained by solving the Helmholtz equation or Master equation

$$\vec{\nabla} \times \left(\frac{1}{\epsilon_r}\right) \vec{\nabla} \times \vec{H} = \left(\frac{\omega^2}{c^2}\right) \vec{H} \quad (2.29)$$

The transfer matrix method (TMM) is used to calculate by layer interactions of electric field and magnetic field vectors at each dielectric medium especially periodic media. Generally, 2x2 TMM is used to study the dispersion behavior and optical properties (reflection and transmission) of 1-DPCs composed of the isotropic layer, which is equivalent to the Fresnel's equations for reflection and transmission coefficients [4].

2.2.1 2x2 Characteristic Matrixes for Single Layer: Consider an electromagnetic plane wave incident on the isotropic homogeneous dielectric layer having relative dielectric permittivity and relative magnetic permeability (ε, μ) with finite thickness. The plane wave has two independent modes for propagations; transverse electric (TE) as well as transverse magnetic (TM) transmission modes. In the TE mode, the electric field components perpendicular to the incident plane wave, while in the case of TM modes, the magnetic

field is perpendicular to the incident plane wave. If the wave propagates in the z-direction and x-y plane is the incident plane wave, then the electric field can be represented as; (i) E=(0, Ey, 0) for TE mode and (ii) E=(Ex, 0, Ez) for TM mode.

The magnetic field and electric displacement vector can be represented by $B = \mu_o \mu H$ and $D = \varepsilon_o \varepsilon E$ for the material's medium.

$$\nabla \times E = -\frac{\partial B}{\partial t} \tag{2.30}$$

$$\nabla \times H = \frac{\partial D}{\partial t} \tag{2.31}$$

On putting the values B and D in equations (2.30) and (2.31) gives;

$$\nabla \times E = i\omega \mu_o \mu H \tag{2.32}$$

$$\nabla \times H = -i\omega \varepsilon_o \varepsilon E \tag{2.33}$$

where ω is the frequency of plane wave and the TE mode polarization, Ey is the y-component of electric field. Therefore, the equation (2.32) gives as;

$$\frac{\partial E_y}{\partial z} = -i\omega \mu_o \mu H_x \tag{2.34}$$

$$0 = i\omega \mu_o \mu H_y \tag{2.35}$$

$$\frac{\partial E_y}{\partial x} = i\omega \mu_o \mu H_z \tag{2.36}$$

And the magnetic field has two $H_x \; and \; H_z$ equation (2.33) gives as;

$$\frac{\partial H_x}{\partial z} - \frac{\partial H_z}{\partial x} = -i\omega \varepsilon_o \varepsilon E_y \tag{2.37}$$

$$\frac{\partial H_x}{\partial y} = 0 \tag{2.38}$$

$$\frac{\partial H_z}{\partial y} = 0 \tag{2.39}$$

On solving the equations (2.34) and (2.39), we found the equation for electric field as;

$$\frac{\partial^2 \mathrm{E_y}}{\partial \mathrm{x}^2} + \frac{\partial^2 \mathrm{E_y}}{\partial \mathrm{z}^2} + k^2 \mathrm{E_y} = 0 \tag{2.40}$$

where k=nω/c, n=$\sqrt{\varepsilon\mu}$ and the solution of the equation (2.40) can be written as;

$$\mathrm{E_y} = \mathrm{E_{0y}}\exp\left(i\mathrm{k_x}x - i\omega t\right) \tag{2.41}$$

Similarly, we can obtain the solutions for the magnetic fields as;

$$\mathrm{H_x} = \mathrm{H_{0x}}\exp\left(i\mathrm{k_x}x - i\omega t\right) \tag{2.42}$$

$$\mathrm{H_z} = \mathrm{H_{0x}}\exp\left(i\mathrm{k_x}x - i\omega t\right) \tag{2.43}$$

Now, on putting the values of $\mathrm{E_y}, \mathrm{H_x}$ and $\mathrm{H_z}$ in the equations (2.34), (2.36), (2.37) and further on solving the equations that gives;

$$\frac{\mathrm{d^2E_{0y}}}{\mathrm{dz^2}} + k_z^2\mathrm{E_{0y}} = 0 \tag{2.44}$$

$$\frac{\mathrm{d^2H_{0x}}}{\mathrm{dz^2}} + k_z^2\mathrm{H_{0x}} = 0 \tag{2.45}$$

The equations (2.44) and (2.45) have solutions as;

$$E_{0y} = A_1 sin(k_z z) + A_2 cos(k_z z) \tag{2.46}$$

$$H_{0x} = \frac{A_1 k_z}{i\omega\mu_0\mu} cos(k_z z) - \frac{A_2 k_z}{i\omega\mu_0\mu} sin(k_z z) \tag{2.47}$$

For TE mode, we can construct a column vector consisting tangential elements of field vectors, which is given as;

$$\Psi(z) = \begin{bmatrix} E_{0y} \\ H_{0x} \end{bmatrix} \tag{2.48}$$

Similar, we can write the field vectors for TM mode;

$$\Psi(z) = \begin{bmatrix} H_{0y} \\ E_{0x} \end{bmatrix} \tag{2.49}$$

The incident electromagnetic wave can be coupled between two planes by a matrix based on solutions of Maxwell's equations that is given as;

$$\Psi(z) = M\Psi(z_0) \tag{2.50}$$

where M is the characteristics matrix of the material, which connects the field vectors at the interface of the materials from z_0 to z. By applying the boundary conditions and further solving, we get the characteristics matrix M that can be written as;

$$M = \begin{bmatrix} \cos(k_z d) & isin\frac{(k_z d)}{p} \\ \text{ipsin}(k_z d) & \cos(k_z d) \end{bmatrix} \tag{2.51}$$

where p=n cosθ for TE mode and p=cosθ/n for TE mode. Using the equation (2.51), we can construct the total transfer matric for one-dimensional periodic structure [3].

2.2.2 Total Transfer Matrix for 1-D Photonic Crystal: We consider 1-D photonic crystal of N layers of dielectric layers of thickness 'a' and 'b' with d periodicity of the periodic structure then d=a+b as shown in the Fig. 2.1.

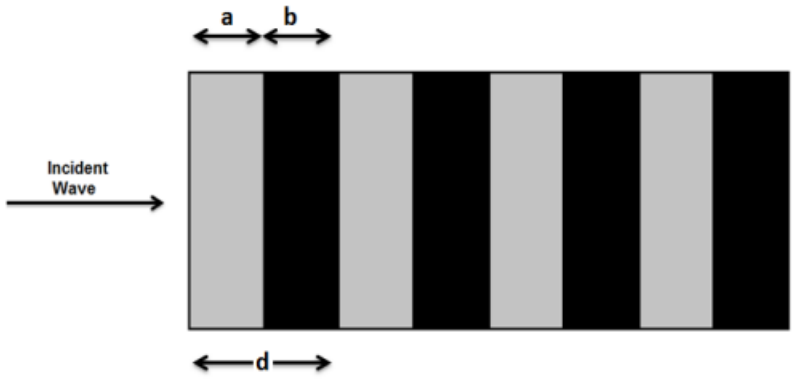

Figure 2.1: Schematic arrangement of 1-DPC of alternating layers of thickness 'a' and 'b' with periodicity d.

Again we consider the vector consisting of electric field and magnetic field elements at the interface of i^{th} layer can be related to the boundary of $(i-1)^{th}$ layer through a matrix M_{i-1} as;

$$\Psi(z_i) = M(z_i - z_{i-1})\,\Psi(z_{i-1}) \tag{2.52}$$

Thus, for N dielectric layers, the final characteristics matrix is the product of all characteristic's matrix of each layer in the structure as;

$$\Psi(z_N) = M(z_N - z_0)\,\Psi(z_0) \tag{2.53}$$

$$M(z_N - z_0) = M(z_N - z_{N-1}) \ldots \ldots M(z_i - z_{i-1}) \ldots M(z_1 - z_0) \tag{2.54}$$

The dispersion relation can be studied by Bloch's wave number; $K=(1/d)\cos^{-1}(\text{Tr}(M(z_N - z_0))/2)$, where $M(d_j)$ is the characteristics matrix for the j^{th} layer in the periodic structure. The $M(d_j)$ is given as;

$$M(d_j) = \begin{bmatrix} \cos(k_{zj}d_j) & isin\frac{(k_{zj}d_j)}{p_j} \\ ip_j\sin(k_{zj}d_j) & \cos(k_{zj}d_j) \end{bmatrix} \quad (2.55)$$

Using equation (2.55), we can write the total transfer matrix for 1-DPC can be found on solving as;

$$r = \frac{(M_{11}+M_{21}p_s)p_0-(M_{21}+M_{22}p_s)}{(M_{11}+M_{21}p_s)p_0+(M_{21}+M_{22}p_s)} \quad (2.56)$$

$$t = \frac{2p_0}{(M_{11}+M_{21}p_s)p_0+(M_{21}+M_{22}p_s)} \quad (2.57)$$

These 'r' and 't' are also called Fresnel's coefficients. By considering conservation of energy, the total reflectance (R) and transmittance (T) of the 1-DPC can be obtained through the following equations [3,4];

$$R = |r|^2 \quad (2.58)$$

$$T = \frac{p_s}{p_0}|r|^2 \quad (2.59)$$

and the absorption (A) is given as;

$$A=1-T-R \quad (2.60)$$

2.3 Transfer Matrix Method (TMM) for Biosensor

The TMM is used to calculate the sensitivity and detection accuracy of the biosensor especially for SPR and LRSPR based biosensors. The reflectance of the incident TM-polarized light is calculated by the application of the Transfer Matrix Method [40]. In the proposed structure, entire layers are aligned in the z-direction and each separate layer is well-defined by their d_k thinness, n_k refractive index (RI) and ε_k dielectric constant, where k=1,2,3. The tangential EM fields at the initial boundary are fixed as $Z=Z_1=0$; and the relation of tangential EM fields between initial and final boundary $Z=Z_{n-1}$ is followed as [43];

$$\frac{U_1}{V_1} = M\frac{U_{n-1}}{V_{n-1}} \quad (2.61)$$

where V_1 and U_1 are magnetic and electric fields at the boundary of the initial layer, V_{n-1} and U_{n-1} are magnetic and electric at the boundary of n^{th} layer, respectively, also M is the total product of all transfer matrices of the collective n layers in the device construction.

The TMM is used for TM-polarization light and the total matrix M for considered configuration is specified as [44,45];

$$M = \prod_{k=2}^{N-1} M_k = \begin{bmatrix} M_{11} & M_{12} \\ M_{21} & M_{22} \end{bmatrix} \tag{2.62}$$

with

$$M_k = \begin{bmatrix} cos\beta_k & \frac{-isin\beta_k}{q_k} \\ -iq_k sin\beta_k & cos\beta_k \end{bmatrix} \tag{2.63}$$

where

$$q_k = \frac{(\varepsilon_k - n_1^2 sin^2\theta_1)^{1/2}}{\varepsilon_k} \text{ and } \beta_k = \frac{2\pi d_k(\varepsilon_k - n_1^2 sin^2\theta_1)^{1/2}}{\lambda},$$

Here, θ_1 is the angle of incidence of electromagnetic wave on the base of 2S2G glass prism. Using TMM, and we can obtain four elements of electric and magnetic fields in the characteristic's matrix M for periodic layers; M_{11} M_{12} M_{21} and M_{22}. By application of these essentials' components, we can compute the coefficient of total reflection r_p for TM or p-polarization light and the relation is given as follows [46];

$$r_p = \frac{(M_{11} + M_{12}q_n)q_1 - (M_{21} + M_{22}q_n)}{(M_{11} + M_{12}q_n)q_1 + (M_{21} + M_{22}q_n)} \tag{2.64}$$

Lastly, the reflectance R_p of n layers for p-polarization is calculated by;

$$R_p = |r_p|^2 \tag{2.65}$$

The variation in the n_s RI of the sensing medium can lead to alteration in reflectance R and the maximum change in R can yield a maximum sensitivity (S). Therefore, the sensitivity (S) can be defined as follows;

$$S = \frac{dR_p}{dn_s} \tag{2.66}$$

Now, for the proposed SPR sensor we can obtain the detection accuracy (DA) from the resulting reflective curves using full width at half maximum (FWHM) from the reflectance of the layered materials [47];

$$DA = \frac{1}{FWHM} \tag{2.67}$$

From equation (2.67) it is predicated that to get the maximum performance sensor, the DA must be maximum as possible. It is apparent that the detection accuracy is inversely proportion to FWHM, consequently, a finer FWHM will produce a maximum DA. To study the high performance sensing behavior of the biosensors, we use frequently equations (2.65), (2.66), and (2.67).

CHAPTER-3

LONG-RANGE SURFACE PLASMON RESONANCE BIOSENSORS WITH CYTOP/Al/PEROVSKITE AND CYTOP/Al/MoS_2 CONFIGURATIONS

3.0 High Sensing Behavior of Optical Biosensor Based on Photonic Crystal

As discussed earlier in the Chapter-1, the multilayered periodic structures or photonic crystals have the unique properties of the obstructions of finite range of frequencies in transmission region, which are called photonic band gaps (PBGs). Such PBGs are used different applications like optical sensors, biosensors, switches, reflectors, optical filters, etc. Today the photonic crystals are used as the optical sensors due to have ultra-compact size with high accuracy and, high efficiency. So, such optical sensors are highly suitable for photonic integrated circuits as well as others several sensing applications. In addition to this, the research on optical sensors based on photonic crystals is going on due to the tunable bandgap of the photonic crystals. However, the metallic photonic crystals are significance in bio-photonics for the bio-sensing application, sensitivity towards biomaterials due to the enhancement of field for the biological media. A biosensor has the change in biological as well as chemical reactions that is able to notice by a tool or device. Such biosensor is based on the creation of signals in responses to applied data or values; and has possible biological effects applications in the detection and disease monitoring, detection of contamination, and disease markers in bodily fluids.

3.1 Surface Plasmon Resonance (SPR) and Long-Range Surface Plasmon Resonance (LRSPR) Based Sensors

As discussed earlier that a collective oscillation of conduction band electrons that are in resonance with the oscillating electric field of incident light is known as surface plasmon resonance (SPR), which through non-radiative excitation will produce energetic plasmonic electrons. These days the SPR based biosensor devices is used to detect the biomolecules in an analyte in the most widespread ways because the surface electrons on metal are getting encouraged by when light wave falls on the surface of metal at the particular

incidence angle. Consequently, electrons of metal surface become to stimulate by incident photons after that propagate on the metal surface. If both frequency as well as momentum have same in photons excitation, then the surface plasmon polariton are produced. Therefore, the surface plasmon polariton wave are used in SPR biosensor to detect the change in the coupling effects of biomolecules and surface of sensing materials and it is also a kind of optical sensor.

In the surface plasmon polariton of metal-dielectric periodic materials, the vertically confined refracting and propagating electromagnetic waves, called a surface plasmon polariton, are used only as a sensor at the interface between the metal and the dielectric layer or sensing material. The trigger surface plasmon resonance on the metal surface depends on the refractive index (RI) of the material. Such resonance is embedded with the metal surface by considering the constant wavelength and angle of incidence of the light. Therefore, a small change in the optical density (RI) of the sensing media drives the expression of surface plasmon resonance to detect analytes. In the surface plasmon resonance assay, analytes are computed by monitoring the intensity of the scattered field or by tracking changes in the resonance angle; which makes real-time and label-free exposure technology useful in bio-sensing applications. Up to the present time, the variety of SPR biosensors has been advancement technically to determine clinically suitable biomarkers. In addition to this, there are several nanomaterials also used to improve the detection responses of surface plasmon resonance biosensors.

The variation in the concentration of biomolecules in the sensing medium yields a local change in the refractive index in contact of metal surface. This change modified optical density leads to a variable diffusion constant of the SPP and can alternatively be measured by the attenuated total reflection technique where the TM polarized surface plasmon wave is excited by metal thin film. Moreover, the long-range surface plasmon resonance (LRSPR) based prism with metal-dielectric interfaces is embedded in the intermediate layers [34]. Since, many representative studies have been performed based on the LRSPR. Matsubara et al. [35] described to achieve high analysis accuracy for the application of long-range geometry SPR sensor. However, the demand and development of high durability with maximum sensitivity, better detection accuracy (DA) and more optimized LRSPR based sensors are growing fast in this field. Implemented Gold (Au) metal

constituent in the conventional LRSPR based sensors is not able to oxidation easily i.e. Au metal does not react with utmost chemicals. Additionally, Au-based sensors show some inefficient sensing response as well as DA i.e., sensitivity and DA of the devices are very small values [36,37]. In order to achieve high and enhanced sensitivity of a biosensor device, the desirable parameters must be better sensitivity, DA and the more stability than the conventional biosensors.

In this dissertation work, different kinds of metal-MoS_2 and metal-Perovskite LRSPR biosensors have been proposed and compared the optical responses of metal-graphene, metal-MoS_2 and metal-Perovskite LRSPR biosensors. In general, Perovskite materials are widely used in solar cells, photoluminescence converters, microwire lasers, and other fields because the Perovskite ($CH_3NH_3PbBr_3$) material has unique feature of its outstanding photoelectric, thermal and electrical properties. Consequently, $CH_3NH_3PbBr_3$ Perovskite has used in the field of optical LRSPR sensors. Wu et al. [38] investigated the sensitivity of the LRSPR biosensor with Cytop/Al/graphene configuration and found that the sensitivity is enhanced greatly by the introduction of the graphene layer in the LRSPR biosensor configuration. So, we have replaced the graphene with MoS_2 and Perovskite for getting better sensor's parameters and compared with Cytop/Al/graphene configuration, which discuss in the next section.

3.2 Cytop/Al/MoS_2 and Cytop/Al/Perovskite Kretschmann Configurations of LRSPR Sensors

The designed structure of the LRSPR biosensor with a thick film of Cytop of thickness of 2000 nm is shown in Fig.3.1. The Figs. 3.1(b) and (c) are the proposed configurations of Al/MoS_2 and Al/Perovskite based biosensors. All configurations are mounted on the chalcogenide glass (2S2G) prism. Al metal thin film of thickness 15 nm is embedded between Cytop and graphene or MoS_2 or Perovskite material. The various configurations of biosensors, Cytop/Al/graphene, Cytop/Al/MoS_2 and Cytop/Al/Perovskite, are considered with biomolecular recognition component as a sensing medium as shown in the Fig.3.1. Here, the 2S2G glass with the high refractive index of has been used as the coupling prism. The employed excitation light wavelength (λ) for the LRSPR sensing is 633nm. Especially, the thickness of graphene is taken (d) i.e., d= N x 0.34 nm, where N means number of monolayers of graphene films. In our study, the thicknesses of MoS_2 and

perovskite are taken the same as the thickness of the graphene. The TM-polarized electromagnetic (EM) wave is incident on one adjacent side of the 2S2G glass prism and after excitation of the EM wave with the considered configurations; the resultant reflective EM wave is detected on the same side through a photodetector i.e., ATR method Kretschmann configuration [38].

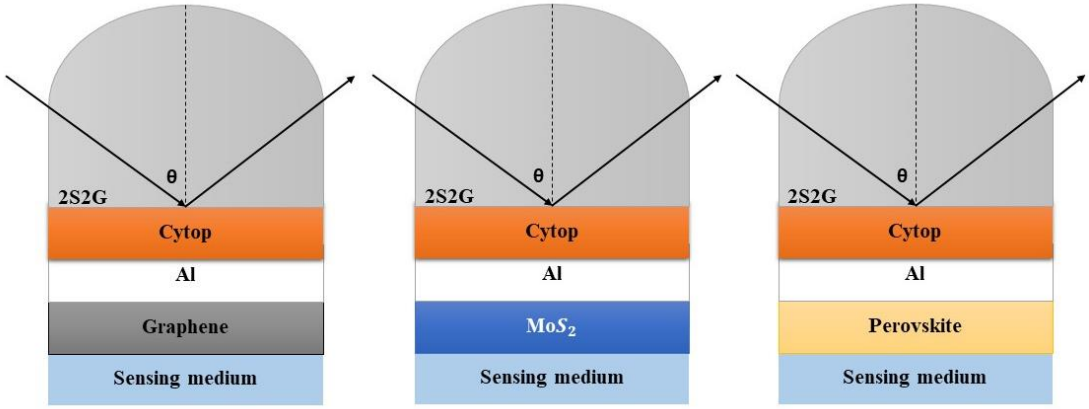

(a) (b) (c)

Figure 3.1: Schematic diagram of LRSPR biosensors with configurations of (a) cytop/Al/graphene, (b) cytop/Al/MoS_2 and (c) cytop/Al/Perovskite.

The refractive index (n_1) of the 2S2G prism is taken as [39];

$$n_1 = 2.24047 + \frac{2.693\times10^{-2}}{\lambda^2} + \frac{8.08\times10^{-3}}{\lambda^4} \tag{3.1}$$

where λ is understand for wavelength of incident EM wave in micrometers. Subsequent, the sensing medium of n_s=1.33 at λ=633 nm is considered due to the very small difference between RI of Cytop thin-layer (n_c=1.34), and such periodic arrangement leads to excite LRSPPs in the metallic interface. Furthermore, the dielectric constant of the Al metal layer is, according to the Drude–Lorentz model, given as [40];

$$\varepsilon_m = 1 - \frac{\lambda^2\lambda_c}{{\lambda_p}^2(\lambda_c + i\lambda)} \tag{3.2}$$

where λ_p and λ_c denote the wavelengths of plasma and collision respectively. The values of λ_p and λ_c for aluminum (Al) are 1.0657×10^{-7}m and 2.4511×10^{-5}m respectively. The RI of graphene in observable range is specified by the formula [41] that is given as;

$$n_g = 3.0 + iC_1\lambda/3; \quad (3.3)$$

where $C_1 \approx 5.446\ um^{-1}$, while λ is the vacuum wavelength in micrometers.

As discussed in the Chapter-2, the reflectance R_p of n layers for p-polarization is calculated using TMM, which is given as;

$$R_p = |r_p|^2 \quad (3.4)$$

As we know that the RI changing of the sensing medium can lead to alteration in reflectance R with variation in the sensing medium (n_s). The maximum sensitivity (S) can be obtained with maximum change in yield reflectance (R). Therefore, the sensitivity (S) is defined as;

$$S = \frac{dR_p}{dn_s} \quad (3.5)$$

Now, the detection accuracy (DA) for the proposed SPR sensor can be obtained from the resulting reflective curves using Full Width at Half Maximum (FWHM) of the reflectance of the layered materials [47]. The DA is given as;

$$DA = \frac{1}{FWHM} \quad (3.6)$$

From equation (3.6), the DA must be the maximum for getting the maximum performance sensor. However, the detection accuracy is inversely proportion to FWHM. Therefore, a finer FWHM will produce a maximum DA.

3.3 Results and Discussion

The LRSPR biosensor consisting different configurations with aluminum metal layer was proposed as shown in the Fig. 3.1 and the sensitivity of the considered LRSPR biosensors was studied and the sensitivities are compared with the conventional metal-graphene LRSPR biosensor. If the materials loss is low, then the sensitivity of the LRSPR sensors is enhanced because the propagation distance and penetration depth of surface plasmon polaritons are longer and deeper than other metals. Besides this, Al is the low-cost material as well as minimum internal damping than the other plasmonic materials [40,59]. Al better-satisfied surface plasmon resonance (SPR) condition in the Kretschmann configuration, the sensitivity and detection accuracy of such configurations are better than the silver and other plasmonic materials. Now the proposed LRSPR biosensors based on Al/graphene or

Al/MoS_2 or Al/Perovskite layers can be used for biomolecular recognition element. For our calculation convenience, we have taken the complex refractive index of MoS_2 and $CH_3NH_3PbBr_3$ Perovskite is 5.2227+1.0804*i and 2 + 0.003*i at λ = 633nm respectively [48-52]. The fluorine-containing insulating polymer, poly-perfluoro-butenyl-vinyl-ether (called Cytop), is used as a small refractive index (RI) layer in the LRSPR sensor [53]. The Cytop is an amorphous material and transparent fluoropolymer through maximum solubility and the film-forming virtues of Cytop at room temperature is also frequently considered as the insulating film in field-effect transistors [54]. Furthermore, the RI of Cytop is taken 1.34 (n_1) at λ = 633 nm, which is extensively used as matching film in SPR sensor [55].

The reflectance (R), sensitivity (S), detection accuracy (DA) and other properties of designed structure at different parameters are studied in the four subsections. In the first subsection, we have studied the reflectance and sensitivity properties by using the TMM for TM mode. In the second subsection, we have studied the variation of reflectance with the variation of RI of sensing medium. In the third subsection, we have studied the sensitivity variation by variation of layer or width of layer. The FWHM and DA of the considered configurations have studied in the last subsection.

3.3.1 Reflectance and sensitivity of different configurations of considered biosensor: The reflectance and sensitivity of designed structure are calculated by using TMM method for EM wave with wavelength 633 nm and RI of sensing medium n_s=1.33. Fig. 3.2 shows the variation of reflectance vs. incident angle for different biosensor configurations. The reflectance of Al based sensors for all combinations (Al-graphene or Al-MoS_2 or Al-Perovskite) are compared. The black curve shows the variation of reflectance regarding incident angle for combination of Aluminum-graphene layer as a conventional LRSPR optical biosensor. The red curve and blue curve show the variation of reflectance versus incident angles for corresponding Al-Perovskite layer and Al-MoS_2 layer configurations respectively. In comparison of the all reflectance, the reflectance for Al-MoS_2 is found zero at the 34.692^o resonance angle and this is most fruitful and suitable configuration for high efficiency and high accuracy LRSPR biosensor.

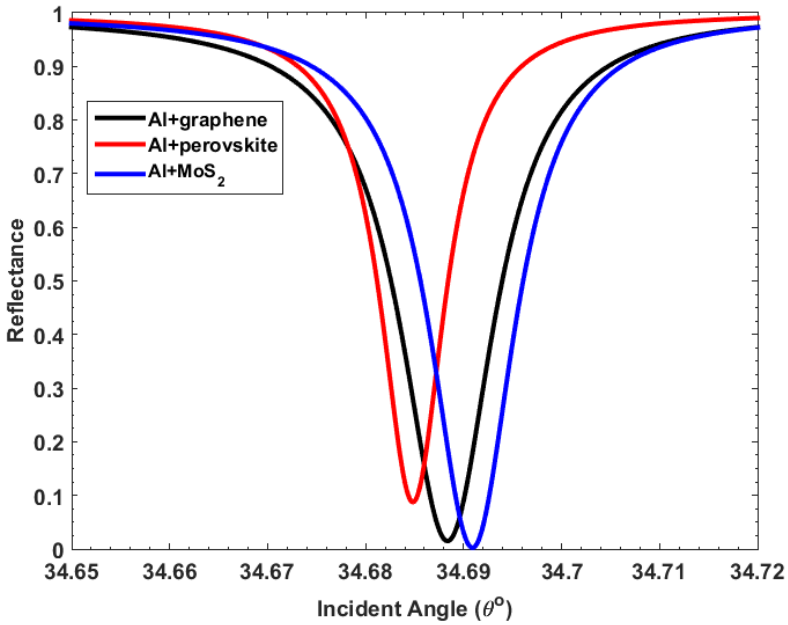

Figure 3.2: Reflectance of the designed biosensors as a function of incident angle for the configurations of Al+different materials.

In Fig. 3.3, the sensitivity versus incident angle has been shown, the black, red and the blue curves represent the sensitivity of Al-graphene, Al-Perovskite and Al-MoS_2 layers, respectively. Depending on the surroundings and angle of incidence the peak sensitivity for the configuration of Al-graphene layer is found to be 1430 RIU^{-1} at 34.69^o resonance angle. Similarly, peak sensitivity for the configuration of Al-Perovskite and Al-MoS_2 layers are found to be 1857.6 RIU^{-1} at 34.68^o resonance angle and 1571.6 RIU^{-1} at 34.69^o resonance angle respectively. From the above results, it is evident that the proposed LRSPR biosensors with the configuration of Al metal layer and Perovskite layer combination have higher peak sensitivity in comparison to the others LRSPR biosensor configurations.

3.3.2 Reflectance with the variation of RI of sensing medium (n_s): The reflectance at 633 nm wavelength is studied with the variation of n_s for all configurations. Now, Figs. 3.4, 3.5 and 3.6 show the reflectance versus resonance angle for the configurations of Al+graphene, Al+Perovskite, and Al+MoS_2 layers respectively with the variation of refractive indices of sensing medium n_s range from 1.3300 to 1.3345.

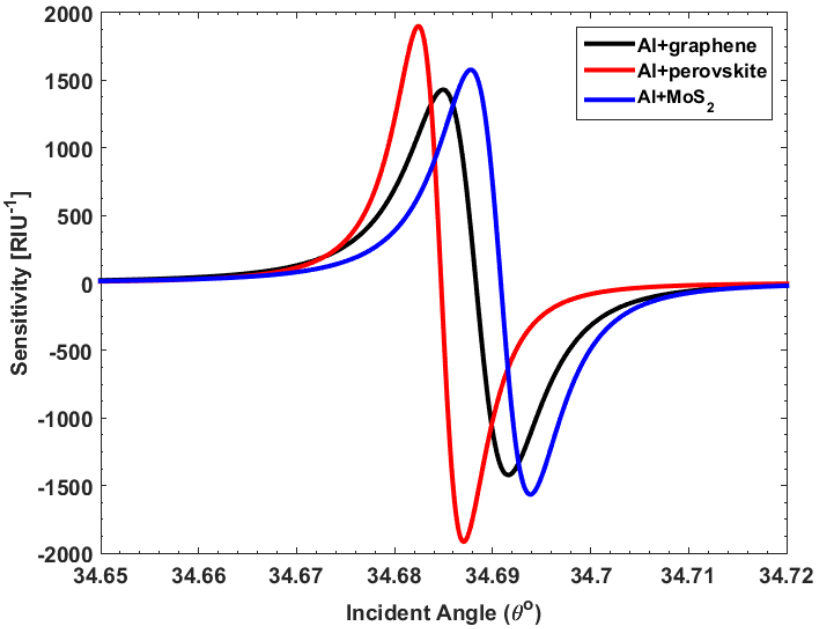

Figure 3.3: Sensitivity of the designed biosensors as a function of incident angle for the configurations of Al+different materials.

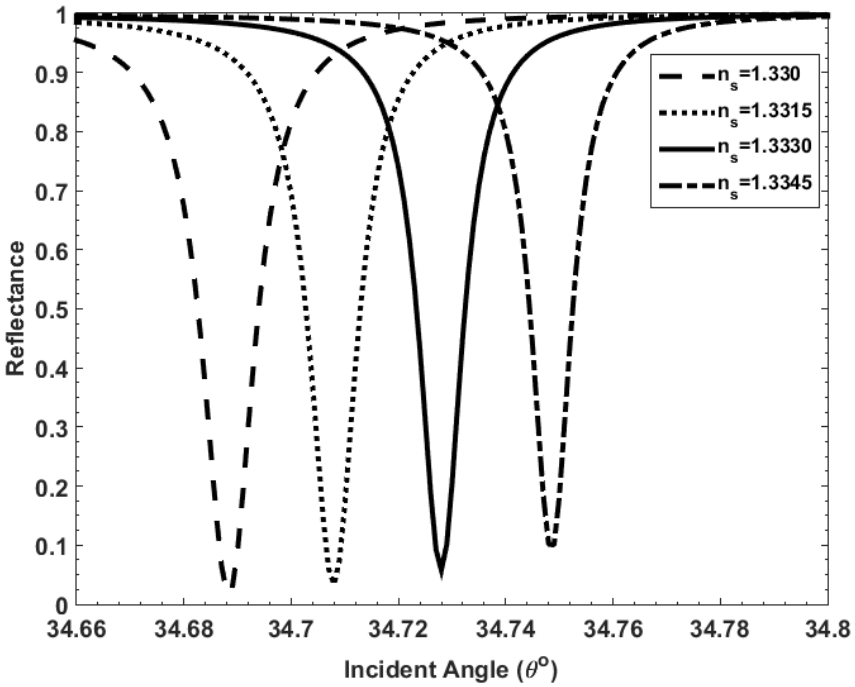

Figure 3.4: Reflectance of the designed Al+graphene biosensor as a function of incident angle by variation of n_s.

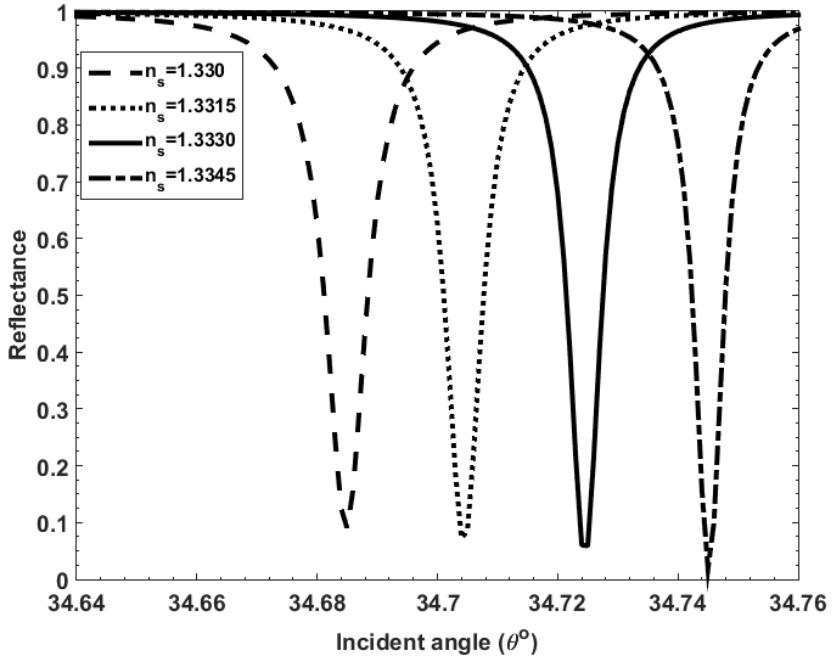

Figure 3.5: Reflectance of the designed Al+Perovskite biosensor as a function of incident angle by variation of n_s.

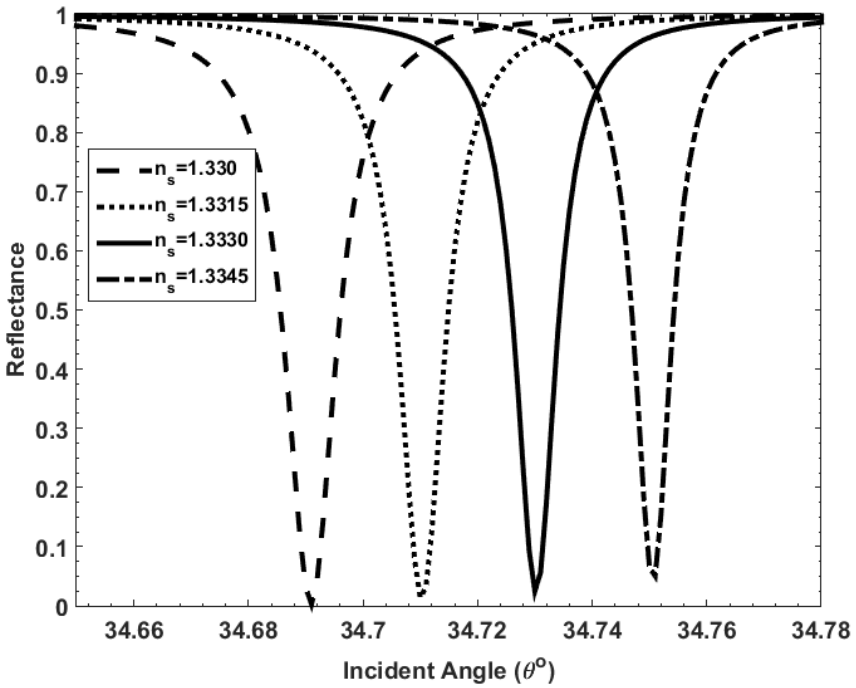

Figure 3.6: Reflectance of the designed Al + MoS_2 biosensor as a function of incident angle by variation of n_s

3.3.3 Peak sensitivity variation with layers or thicknesses and refractive indices: The peak sensitivity of the considered LRSPR biosensors is varied with number of layers and thicknesses of the sensing material. Peak sensitivity is an important factor to influence the performance of the proposed biosensor. The Fig. 3.7 demonstrates the variation of maximum sensitivity with respect to the number of layers for the proposed LRSPR biosensor based on Al-graphene, Al-MoS_2 and Al-perovskite for 633 nm source wavelength and 1.33 sensing medium RI. The thickness of the graphene, MoS_2 and perovskite layer is taken as N×0.34 nm, where N is number of layers. For Al-graphene layer configuration, the black line shows the variation of peak sensitivity by increasing the number of graphene layers. The maximum peak sensitivity for Al-graphene configuration with single layer of graphene is to be found 1430 RIU^{-1}. Similarly, the blue line shows the peak sensitivity of the Al-MoS_2 configuration for variation of MoS_2 layers and the red line shows the peak sensitivity of Al-Perovskite, which is increased with increase the thickness of the MoS_2 and Perovskite i.e., increase number of graphene layers. The thickness of MoS_2 and Perovskite is equal to the multiple of 0.34nm to number of layers. The maximum peak sensitivity of the biosensor is found 1571 RIU^{-1} for single layer MoS_2 layer. This result reveals that the single layer of the graphene and MoS_2 shows maximum sensitivity, but the synthesis of the single layer of graphene or MoS_2 layer is very complicated. Therefore, we would look into another material like Perovskite that is used in many devices. So, Perovskite materials can be used for simple synthesis for LRSPR biosensor and sensitivity may be high due to its easily transport of charge carriers. In the study, reflectance and peak sensitivity of the configuration of Al-Perovskite layer has found to be 1857.6 RIU^{-1} at 34.68^{o} for the thickness 0.34 nm, which better than another configuration. So, we have emphasized on the LRSPR biosensor based on the Perovskite layer as sensing material and studied the peak sensitivity by variation of width of Perovskite layer.

The peak sensitivity of Al-Perovskite configuration is increased with increase of the thickness of the Perovskite layer. Fig. 3.8 shows the variation of peak sensitivity by variation of thickness of perovskite layer for Al-Perovskite configuration LRSPR biosensor.

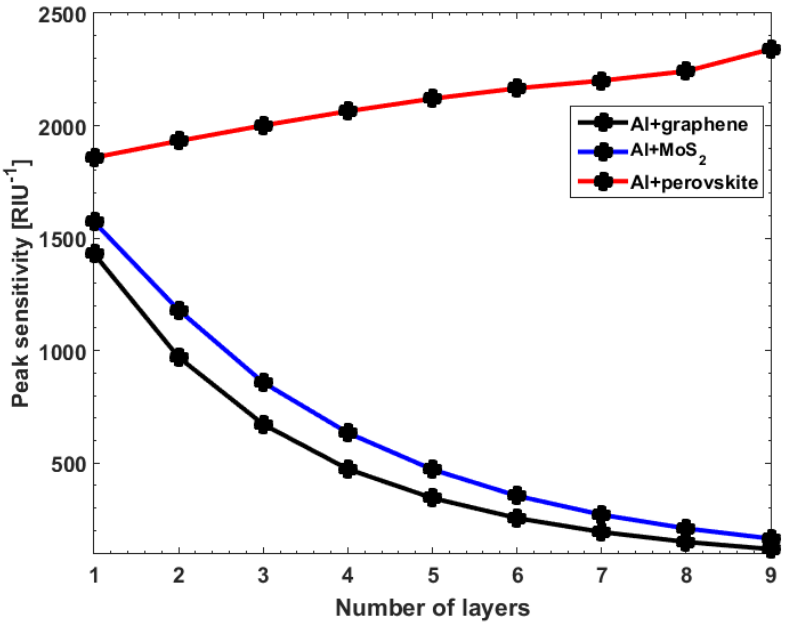

Figure 3.7: Peak sensitivity of designed structure at different number of layers (N) where the thickness of materials for all configurations is Nx0.34 nm.

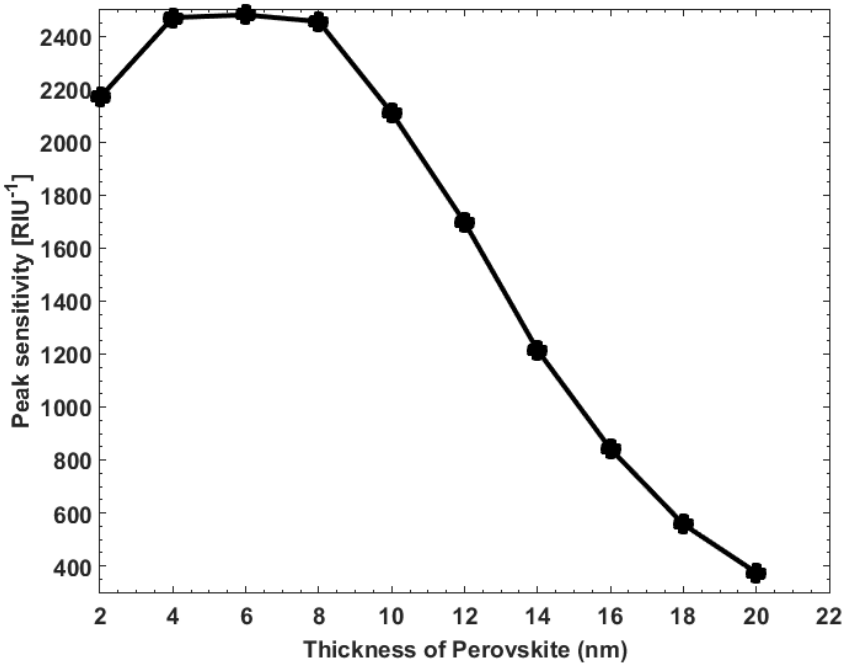

Figure 3.8: Peak sensitivity of designed structure at different thicknesses (nm) of the perovskite.

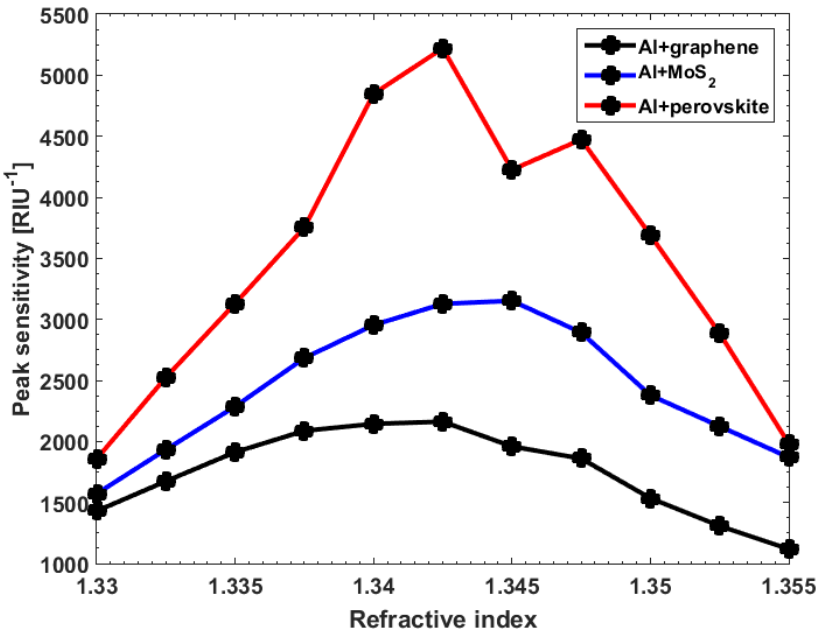

Figure 3.9: Peak sensitivity vs. refractive index of sensing medium for all configurations

The peak sensitivity of Al-Perovskite is increased firstly with increases thickness of Perovskite layer up to 8nm and then it is started to decrease with increases thickness of Perovskite layer above 8nm. The maximum peak sensitivity is found to be 2482 RIU^{-1} for 6.5 nm thickness of Perovskite layer at λ=633 nm and n_s= 1.33.

Fig. 3.9 shows the variation of peak sensitivity versus RI of sensing medium n_s. The black curve, the blue curve and the red curve are the variation of peak sensitivity of Aluminum-graphene, Aluminium-MoS_2 and Aluminum-Perovskite respectively with thickness of Aluminum is fixed i.e., 15nm and thicknesses of other materials are taken equivalent to single layer graphene i.e., 0.34 nm. Here, it is inferred that the peak sensitivity for graphene, MoS_2 and Perovskite layer is increased by n_s; but the sensitivity of Perovskite layer, in comparison to both materials, is increased sharply by increasing n_s and found to be the maximum value 5220 RIU^{-1} at 34.87^o for n_s =1.3425. After this maximum value of the sensitivity, it starts to decrease. This result reveals that the peak sensitivity of the Al-

Perovskite configuration has best for the sensing medium of refractive index around 1.3425.

3.3.4 Variation of Full Width Half Maxima (FWHM) and Detection Accuracy (DA): For the LRSPR biosensors, the FWHM (Fig. 3.10) and DA (Fig. 3.11) are also the important factors to show the performance of the biosensor as increase the thickness of the sensing materials. Due to the high absorbing layers, the dip of the LRSPR reflectance curve will get finer and the FWHM will be widen. However, the DA of the LRSPR is the reciprocal of the FWHM. The studies show that the DA of the Perovskite material is found very high in comparison to the others materials because the FWHM is very low for Perovskite material. Moreover, the resonance angle of LRSPR reflectance curve alters from low to high angles with the increase of layers as shown in the Fig. 3.12. A comparative table 3.1 for sensitivity of the biosensor with different configurations is given and indicates that the sensitivity of proposed Al-MoS_2 and Al-Peroskite based LRSPR biosensors has found nearly 10% and nearly 30% more sensitive than the standard Al-graphene LRSPR biosensor.

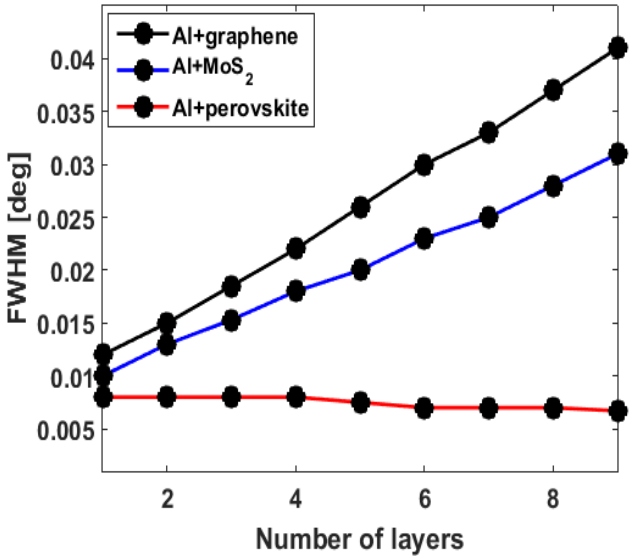

Figure 3.10: Variation of FWHM with number of layers at different configuration of periodic layers.

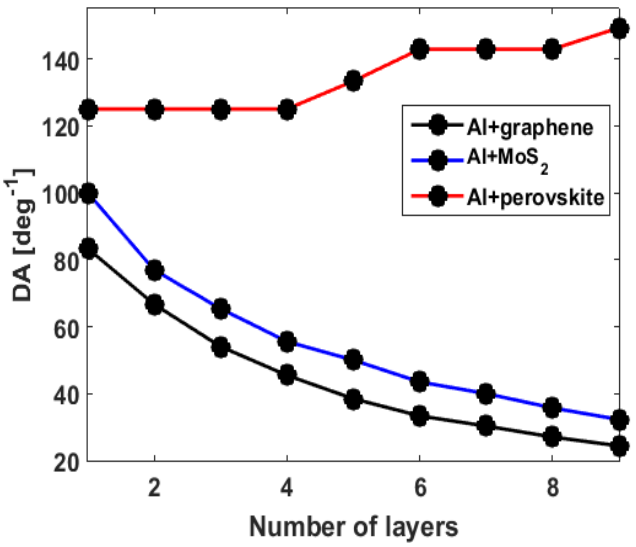

Figure 3.11: Detection accuracy (DA) vs layers

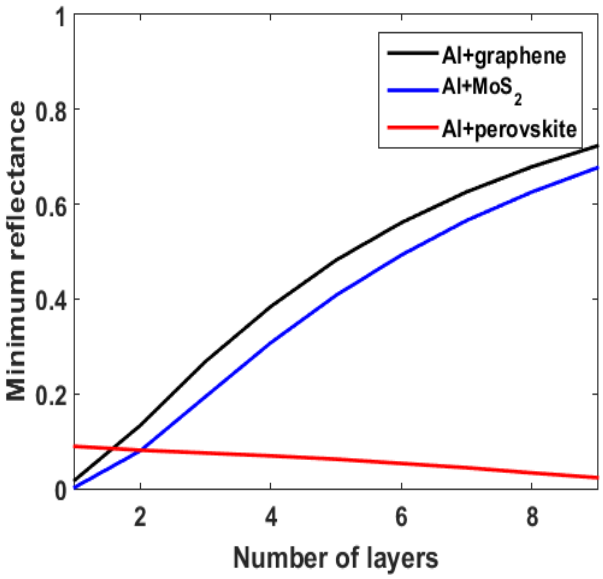

Figure 3.12: Minimum reflectance vs. thickness of materials (~L × 0.34nm), where L is number of layers

Table 3.1: Comparative table for sensitivity of the biosensor with different configurations

Configuration	Sensitivity	Reference
Al + perovskite	1857.6 RIU^{-1}	Our result [60]
Al + MoS_2	1571.6 RIU^{-1}	Our result [60]
Al + graphene	1430.0 RIU^{-1}	[47]
Graphene/Ag-based SPR sensor	455.4 RIU^{-1}	[56]
TMDCs/Al-based SPR sensor	895.6 RIU^{-1}	[57]
TMDCs/Au-based LRSPR biosensor	1240.2 RIU^{-1}	[58]

3.4 Conclusion and Future Scope

In this dissertation work, we have proposed a new configuration of LRSPR biosensors based on the Al-MoS_2 and Al-Perovskite. The proposed confugations have found the enahanced sensitivity and high detection accuracy in comparison to conventional Al-graphene LRSPR biosensor. However, the sensitivity of proposed LRSPR biosensor based on the Al-Perovskite with thickness of Perovskite material 0.34 nm has highest peak sensitivity (4847 RIU^{-1}) for sensing medium of RI 1.34, which is highest value for the LRSPR biosensors. Moreover, the sensitivity of proposed Al-MoS_2 based LRSPR biosensor is nearly 10% more sensitive than the standard Al-graphene LRSPR biosensor, while Al- Perovskite based with same congiuration type have nearly 30% more sensitive than the standard Al-graphene LRSPR biosensor.

The calculated results reveal that the enhanced sensitivity of nearly 30% Al-Perovskite and nearly 10% Al-MoS_2 based LRSPR biosensors more than the conventional Al-graphene LRSPR biosensor may be used for high performance sensing devices. Hence, the proposed LRSPR bisosensors may be useful to detect biomolecules as well as surface plasmon resonance imaging (SPRI). The SPRI may be used in several applications of biomedical, proteomics, genomics and bioengineering fields. In future, the high performance sensing devices of Al-Perovskite based LRSPR bisosensor and Al-MoS_2 based LRSPR bisosensor may be fabricated for practical realization to biomolecules detecting as well as surface plasmon resonance imaging by low cost synthesis or fabrication methods.

REFERENCES

[1] A. Ghatak, Optics, Tata McGraw-Hill, New Delhi, 2008.

[2] D. J. Griffiths, Introduction to Electrodynamics, Prentice Hall, Upper Saddle River, New Zersey, USA, 1999.

[3] P. Yeh, Optics in Layered Media, John Willey and Sons, New York, 1988.

[4] J. D. Joannopolos, S. G. Johnson, J. N. Winn and R. D. Meade, Photonic crystals: Molding the flow of light, Second Edt., Princeton NJ, USA, 2008. http://ab-initio.mit.edu/book/photonic-crystals-book.pdf

[5] A. Sopaheluwakan, Thesis on Defect States and Defect modes in 1D photonic crystals, Uppsala Univ. Swedon, 2005.

[6] E. Yabolonovitch, Inhibited spontaneous emission in solid state physics and electronics, Phys. Rev. Lett. 58, 2059-2062, 1987.

[7] S. John, Strong localization of photons in certain disordered dielectric super lattices, Phys. Rev. Lett. 58, 2486-2489, 1987.

[8] Y. Fink, J. N. Winn, S. Fan, C. Chen, J. Michel, J. D. Joannopoulos, E. L. Thomas, A dielectric omnidirectional reflector, Science 282, 1679–1682, 1998.

[9] F. Wu, K. Lyu, S. Hu, M. Yao, S. Xiao, Ultra-large omnidirectional photonic band gaps in one-dimensional ternary photonic crystals composed of plasma, dielectric and hyperbolic metamaterial, Opt. Mater. 111, 110680, 2021.

[10] F. Wu, X. Wu, S. Xiao, G. Liu, H. Li, Broadband wide-angle multilayer absorber based on a broadband omnidirectional optical Tamm state, Opt. Exp. 29, 23976–23987, 2021.

[11] T. F. Krauss, RM D. L. Rue and S. Brand, Two-dimensional photonic bandgap structures operating at near infrared wavelengths, Nature 383, 699-702, 1996.

[12] J. D. Joannopoulos, P. R. Villeneuve, S. Fan, Photonic crystals: putting a new twist on light, Nature 386, 143–149, 1997.

[13] H. Inan, M. Poyraz, F. Inci, M. A. Lifson, M. Baday, B.T. Cunningham, U. Demirci, Photonic crystals: emerging biosensors and their promise for point-of-care applications, Chem. Soc. Rev. 46, 366–388, 2017.

[14] C. Fenzl, T. Hirsch, O. S. Wolfbeis, Photonic crystals for chemical sensing and biosensing, Angew. Chem. Int. Ed. Engl. 53, 3318–3335, 2014.

[15] H. Chen, R. Lou, Y. Chen, L. Chen, J. Lu, Q. Dong, Photonic crystal materials and their application in biomedicine, Drug Deliv. 24, 775–780, 2017.

[16] R. Rajasekar, S. Robinson, Photonic Crystal-Based Sensors for Biosensing Applications, Book: Advances in Photonic Crystals and Devices, N. Kumar and B. Suther (Editors), CRC Publ., ISBN 9781138552463, 2019.

[17] D. M. El-Amassi, S.A. Taya, D. Vigneswaran, Temperature sensor utilizing a ternary photonic crystal with a polymer layer sandwiched between Si and SiO_2 layers, J. Theor. Appl. Phys. 12, 293–298, 2018.

[18] B.K. Singh, P.C. Pandey, Effect of temperature on terahertz photonic and omnidirectional band gaps in one-dimensional quasi-periodic photonic crystals composed of semiconductor InSb, Appl. Opt. 55, 5684–5692, 2016.

[19] T-W. Lu, C-C. Wu, P-T. Lee, 1D photonic crystal strain sensors, ACS Photonics 5, 2767–2772, 2018.

[20] N. R. Ramanujam, I. S. Amiri, S. A. Taya, S. Olyaee, R. Udaiyakumar, A. P. Pandian, K. S. J. Wilson, P. Mahalakshmi, P. P. Yupapin, Enhanced sensitivity of cancer cell using one dimensional nano composite material coated photonic crystal, Microsystem. Technol. 25, 189–196, 2019.

[21] S. A. Maier, Plasmonics: Fundamentals and Applications, Springer, 2007, ISBN: 978-0-387-33150-8.

[22] H. Emami Nejad, A. Mi, A. Farmani, Supersensitive and tunable nano biosensor for Cancer detection, IEEE Sens. J., 19, 4874-4881, 2019.

[23] H. J. El-Khozondar, P. Mahalakshmi, R. J. El-Khozondar, N. R. Ramanujam, I. S. Amiri, P. Yupapin, Design of one dimensional refractive index sensor using ternary photonic crystal waveguide for plasma blood samples applications, Physica E: Low-dim. Syst. Nanostr. 111, 29–36, 2019.

[24] H. Raether, Surface Plasmons on Smooth and Rough Surfaces and on Gratings. Berlin, Germany: Springer-Verlag, 1988, ISBN: 978-3-540-47441-8.

[25] E. Hutter, J. H. Fendler, Exploitation of Localized Surface Plasmon Resonance, Adv. Maters. 16, 1685–1706, 2004.

[26] W. Hickel, D. Kamp, W. Knoll, Surface-plasmon microscopy, Nature, 339, 186, 1989.

[27] Y. Gao, Z. Xin, B. Zeng, O. Gan, X. Cheng, F. J. Bartoli, Plasmonic interferometric sensor arrays for high-performance label-free biomolecular detection, Lab on a Chip, 13, 4755–4764, 2013.

[28] A. Barik, L. M. Otto, D. Yoo, J. Jose, T. W. Johnson, S-H. Oh, Dielectrophoresis-Enhanced Plasmonic Sensing with Gold Nanohole Arrays, Nano Lett., 14, 2006–2012, 2014.

[29] B. Zeng, Y. Gao, F. J. Bartoli, Rapid and highly sensitive detection using Fano resonances in ultrathin plasmonic nanogratings, Appl. Phys. Lett., 105, 161106, 2014.

[30] B. Zeng, Y. Gao, F. J. Bartoli, Differentiating surface and bulk interactions in nanoplasmonic interferometric sensor arrays, Nanoscale, 7, 166–170, 2015.

[31] X. Dai, L. Jiang, Y. Xiang, Low threshold optical bistability at terahertz frequencies with graphene surface plasmons, Sci. Rep., 5, 12271, 2015.

[32] X. Dai, L. Jiang, Y. Xiang, Tunable THz Angular/Frequency Filters in the Modified Kretschmann–Raether Configuration with the Insertion of Single Layer Graphene, IEEE Photon. J., 7, 5500808, 2015.

[33] K. Johansen, H. Arwin, I. Lundstrõm, B. Liedberg, Imaging surface plasmon resonance sensor based on multiple wavelengths: Sensitivity considerations, Rev. Sci. Instrum., 71, 3530–3538, 2000.

[34] D. Sarid, Long-Range Surface-Plasma Waves on Very Thin Metal Films, Phys. Rev. Lett., 47, 1927–1930, 1981.

[35] K. Matsubara, S. Kawata, S. Minami, Multilayer system for a high-precision surface plasmon resonance sensor, Opt. Lett., 15, 75–77, 1990.

[36] O. Krupin, H. Asiri, C. Wang, R. N. Tait. P. Berini, Biosensing using straight long-range surface plasmon waveguides, Opt. Exp., 21, 698–709, 2013.

[37] J. C. Love, L. A. Estroff, J. K. Kriebel, R. G. Nuzzo, G. M. Whitesides, Self-assembled monolayers of thiolates on metals as a form of nanotechnology, Chem. Rev., 105, 1103–1169, 2005.

[38] L. Wu, Z. Ling, L. Jiang, J. Guo, X. Dai, Y. Xiang, D. Fan, Long-Range Surface Plasmon With Graphene for Enhancing the Sensitivity and Detection Accuracy of Biosensor, IEEE Photonics J., 8, 4801409, 2016.

[39] P. K. Maharana, R. Jha, Chalcogenide prism and graphene multilayer based surface plasmon resonance affinity biosensor for high performance, Sensors and Actuators: B. Chem., 169, 161–166, 2012.

[40] A. K. Sharma, B. D. Gupta, On the performance of different bimetallic combinations in surface plasmon resonance based fiber optic sensors, J. Appl. Phys., 101, 093111, 2007.

[41] M. Bruna, S. Borini, Optical constants of graphene layers in the visible range, Appl. Phys. Lett., 94, 031901, 2009.

[42] M. Yamamoto, Surface plasmon resonance (SPR) theory: Tutorial, Encyclopedic Reference of Immunotoxicology, 14, 388–398, 2002.

[43] S. Zeng, S. Hu, J. Xia, T. Anderson, X-Q. Dinh, X-M. Meng, P. Coquet, K-T. Yong, Graphene-MoS_2 hybrid nanostructures enhanced surface plasmon resonance biosensors, Sensors and Actuators: B. Chem., 207, 801–810, 2015.

[44] P. K. Maharana, R. Jha, S. Palei, Sensitivity enhancement by air mediated graphene multilayer-based surface plasmon resonance biosensor for near infrared, Sensors and Actuators: B. Chem., 190, 494–501, 2014.

[45] R. Verma, B. D. Gupta, R. Jha, Sensitivity enhancement of a surface plasmon resonance-based biomolecules sensor using graphene and silicon layers, Sensors and Actuators: B. Chem., 160, 623–631, 2011.

[46] L. Wu, H. S. Chu, W. S. Koh, E. P. Li, Highly sensitive graphene biosensors based on surface plasmon resonance, Opt. Express, 18, 14395–14400, 2010.

[47] P. K. Maharana, T. Srivastava, R. Jha, On the performance of Highly Sensitive and Accurate Graphene-on-Aluminum and Silicon-Based SPR Biosensor for Visible and Near Infrared, *Plasmonics*, 9 (5), 1113–1120, 2014.

[48] J. B. Maurya, A. Francois, Y. K. Prajapati, Two-Dimensional Layered Nanomaterial-Based One Dimensional Photonic Crystal Refractive Index Sensor, Sensors, 18, 857, 2018.

[49] https://refractiveindex.info/?shelf=main&book=MoS2&page=Beal, 2022.

[50] A. R. Beal, H. P. Hughes, Kramers-Kronig analysis of the reflectivity spectra of 2H-MoS_2, 2H-$MoSe_2$ and 2H-$MoTe_2$. J. Phys. C: Solid State Phys. 12, 881–890, 1979.

[51] S. Brittman, E. C. Garnett, Measuring n and k at the Microscale in Single Crystals of $CH_3NH_3PbBr_3$ Perovskite, J. Phys. Chem. C 120, 616–620, 2016.

[52] H. Zhang, Y. Ma, Y. Wan, X. Rong, Z. Xie, W. Wang, L. Dai, Measuring the refractive index of highly crystalline monolayer MoS_2 with high confidence, Sci. Rep. 5, 8440, 2015.

[53] Y. Zheng, W. Shi, J. Kong, D. Huang, H. E. Katz, J. Yu, A. D. Taylor, A Cytop Insulating Tunneling Layer for Efficient Perovskite Solar Cells, Small Methods 1, 1700244, 2017.

[54] W. Huang, K. Besar, R. LeCover, P. Dulloor, J. Sinha, J. F. M. Hardigree, C. Pick, J. Swavola, A. D. Everett, J. Frechette, M. Bevan, H. E. Katz, Label-free brain injury biomarker detection based on highly sensitive large area organic thin film transistor with hybrid coupling layer, Chem. Sci. 5, 416–426, 2014.

[55] C. Yue, Y. Lang, X. Zhou, Q. Liu, Sensitivity enhancement of an SPR biosensor with a graphene and blue phosphorene/transition metal dichalcogenides hybrid nanostructure, Appl. Opt. 58, 9411-9420, 2019.

[56] P. K. Maharana, R. Jha, P. Padhy, On the electric field enhancement and performance of SPR gas sensor based on graphene for visible and near infrared, Sensors and Actuators: B. Chem., 207, 117-122, 2015.

[57] Y. Xu, L. Wu, L. K. Ang, MoS_2 Based Highly Sensitive Near-Infrared Surface Plasmon Resonance Refractive Index Sensor, IEEE J. Selected Topics Quant. Electronics, 25, 2, 1-7, 2019.

[58] Y. Xu, C-Y. Hsieh, L. Wu, L. K. Ang, Two dimensional transition metal dichalcogenides mediated long range surface plasmon resonance biosensors, J. Phys. D, 52, 6, 065101, 2019.

[59] Q. Wang, J-Y. Jinga, Z. Cheng, Long-range surface plasmon resonance and its biological sensing applications, Chapter-Eight, Handbook on Comprehensive Analytical Chemistry, 95, 277-338, 2021, ISBN 9780323853095; https://www.sciencedirect.com/science/article/abs/pii/S0166526X21000726.

[60] M. Kumar, K. B. Thapa, P. Singh, Long-range surface plasmon resonance biosensors with cytop/Al/Perovskite and cytop/Al/MoS_2 configurations, Phys. Scr., 97, 055501, 2022.

List of Publication

Mohit Kumar, Khem B. Thapa, Pawan Singh, *Long-range surface plasmon resonance biosensors with cytop/Al/Perovskite and cytop/Al/MoS_2 configurations*, **Phys. Scr**., 97, 055501, 2022.

List of the Conference/Webinar attended/presented

Oral presentation on "*Long-range surface plasmon resonance biosensors with cytop/Al/Perovskite and cytop/Al/MoS_2 configurations*" WEBINAR on '***SCIENCE: In Today's Prospect***' February 28, 2022, organized by Department of Physics, Siddharth University, Kapilvastu (UP) India.

ANNEXURE

(i) Certificate of Oral Presentation

SIDDHARTH UNIVERSITY, KAPILVASTU
DEPARTMENT OF PHYSICS
WEBINAR on 'SCIENCE: In Today's Prospect'
February 28, 2022

CERTIFICATE

This is to certify that **Mohit Kumar**

Affiliation: **Dept. of Physics, Babasaheb Bhimrao Ambedkar University, Lucknow**

~~participated~~/ presented a paper (oral) in the webinar organized by Department of Physics, Siddharth University, Kapilvastu, Siddharthnagar on 28 February, 2022.

Paper Title: **Long-range surface…Al/MoS_2 configurations**

Convener Co-convener Secretary Joint-secretary

(ii) Published paper

Physica Scripta

PAPER

Long-range surface plasmon resonance biosensors with cytop/Al/Perovskite and cytop/Al/MoS_2 configurations

Mohit Kumar, Khem B. Thapa and Pawan Singh

Department of Physics, School of Physical and Decision Science, Babasaheb Bhimrao Ambedkar University (A Central University), Vidya Vihar, Raebareli Road, Lucknow, 226025, India

E-mail: khem.bhu@gmail.com

RECEIVED
12 January 2022

REVISED
15 March 2022

ACCEPTED FOR PUBLICATION
16 March 2022

PUBLISHED
28 March 2022

Keywords: one-dimensional photonic crystal (1-DPC), biosensor, surface plasmon resonance (SPR), transfer matrix method (TMM) and LRSPR biosensors

Abstract

In this paper, long range surface plasmon resonance (LRSPR) biosensors with cytop/Al/Perovskite and cytop/Al/MoS_2 configurations have been theoretically investigated and compared with standard LRSPR biosensor with cytop/Al/graphene configuration. To calculate the optical properties of considered configurations for the desired application, transfer matrix method for TM mode has been used to obtain reflectance. The sensitivity of the considered configurations for designed biosensors has been investigated with variation of optical parameters of the structure. A new configuration of LRSPR biosensors based on Al- MoS_2 or Al-Perovskite has been proposed to enhance sensitivity, detection accuracy, and efficiency. The maximum value of sensitivity of the proposed Al-Perovskite based LRSPR biosensor is found to be 4847 RIU^{-1}. Moreover, the sensitivity of Al-MoS_2 and Al-Peroskite based LRSPR biosensors show nearly 10% and nearly 30% more optical responses respectively than the Al-graphene based LRSPR biosensor.

1. Introduction

To control the flow or propagation of electromagnetic wave in the optical materials, the dielectric function or refractive index is crucial parameter. Generally, a periodic multilayered material shows very special property to control the propagation of electromagnetic wave due to periodicity of the dielectric functions of the materials. Such periodic multilayered structures exhibit frequency ranges in the transmission spectra called photonic band gaps (PBGs), which obstruct the propagation of electromagnetic waves [1–3]. Such multilayered structures are known as photonic crystals [4–6]. The photonic crystals can be used in different optical applications like reflectors, optical filters, switches, biosensors etc [1, 7]. The biosensing application of the photonic crystals is also to have significance in bio-photonics due to field enhancement effects, sensitivity towards biomaterials [7–9]. Basically, a device that detects and responds to specific input from the physical system is called a sensor [10]. Based on the changing physical phenomena, the sensors are classified into various types of sensors like temperature sensor, pressure sensor, optical sensor, microphone sensor, digital sensor, mechanical sensor, biochemical sensor etc [11–17]. In these sensors, the optical sensors have the most durable with high efficiency and high accuracy due to the evanescent field wave phenomenon where the optical sensor is used to monitor in the changing refractive index. The evanescent field occurs within a few hundred nano-meter of the sensor surface [18]. Due to ultra-compact size, high efficiency and high accuracy, the optical sensors are most desirable in the sensing applications having the highly appropriate for photonic integrated circuits [13].

A device or tool detected change in the biological as well as chemical reactions, which is based on the creating signals in responses of applied data or values, is generally known as biosensor. Such biosensors have potential applications in the biological effects as detection and monitoring of disease, contamination detection, and disease markers in bodily fluids [18, 19]. The surface plasmon resonance (SPR) of metal is used in the most popular biosensors. When light wave is incident at a certain angle on metal, then surface electrons on metal get stimulated by incident photons and propagate on the metal surface. When both frequency and momentum have

© 2022 IOP Publishing Ltd

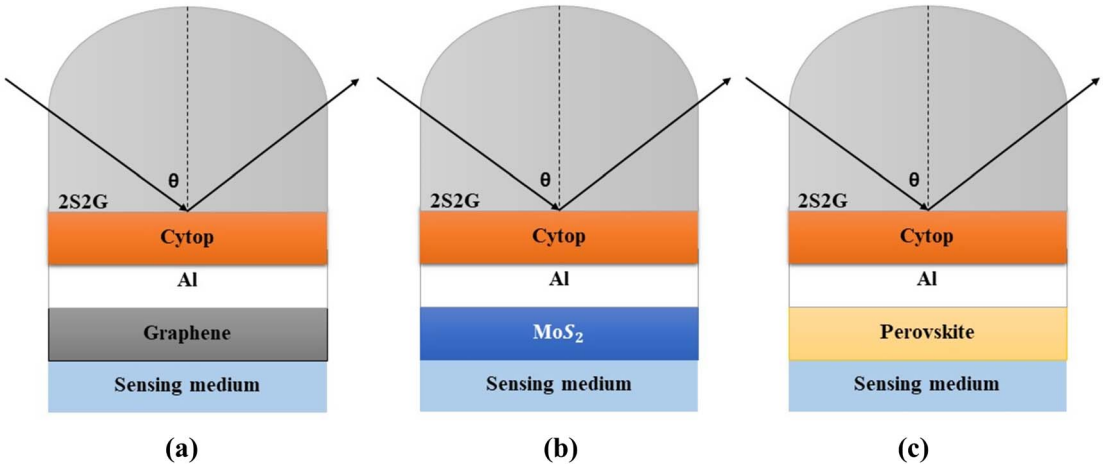

Figure 1. Schematic diagram of LRSPR biosensors with configurations of (a) cytop/Al/graphene, (b) cytop/Al/MoS2 and (c) cytop/Al/Perovskite.

same in the photons excitation, then surface plasmon polariton (SPP) is generated. Hence, SPR biosensor is a type of optical sensor that uses surface plasmon polariton (SPP) waves to detect the changes in the coupling effects of biomolecules and surface of sensing material. In the SPP of metal-dielectric periodic materials, SPP is a vertically confined refracting electromagnetic wave and such propagating waves on the interface between the metal and the dielectric layer (sensing material) easily use as a sensor [15, 18, 19]. By considering constant wavelength and angle of light incidence, the triggered SPR on the metal surface depends on the optical density/refractive index (RI) of the material, which embedded with the metallic surface. Consequently, a small variation in the optical density of the sensing media leads to encumber the manifestation of SPR to detect analytes. In the SPR assay, analytes are quantified by monitoring the scattered field intensity or by tracking the shifting in resonance angle; that makes a real-time and label-free exposure technique and is useful in the bio-sensing applications. So far, a variety of SPR biosensors have been technologically advanced for the detection of clinically appropriate biomarkers. Several nanomaterials are also used to enhance the optical responses of SPR biosensors. The SPR is theoretically is very crucial parameter for real-world applications such as biological analysis devices [20–24], optical bistability devices [25], and THz filters [26]. Furthermore, SPR is extensively employed in detecting devices that SPR sensor offers unique advantages such as real-time analysis and high reliability with very high sensitivity [27].

In the sensing medium, variation in the concentration of biomolecules yields a local change in the refractive index in contact of metal surface. The modified optical density leads to a variable diffusion constant of the SPP and can alternatively be measured by the attenuated total reflection technique. Here, the TM polarized surface plasmon wave is excited by metal thin film, however the long-range surface plasmon resonance (LRSPR) based prism with metal-dielectric interfaces is embedded in the intermediate layers [28]. Since, many representative studies have been done based on the LRSPR. Matsubara *et al* [29] described to achieve high analysis accuracy for the application of long-range geometry SPR sensor. However, the demand and development of high durability with maximum sensitivity, better detection accuracy (DA) and more optimized LRSPR based sensors are growing in this field of interest from last few couple of years. In the conventional LRSPR based sensors, Gold (Au) is implemented as the metal constituent, but it is not able to process oxidation, additionally, it also does not react with utmost chemicals. Besides, these Au-based sensors show some inefficient sensing responses and DA i.e. they are small values [30, 31]. In order to achieve enhanced sensitivity of a biosensor device, the desirable parameters are the better DA and the more stability than the conventional biosensors. Here, we have proposed different kinds of metal-MoS_2 and metal-Perovskite LRSPR biosensors. The sensing behaviors of the proposed biosensors have been studied. Moreover, we have also compared the optical responses of metal-graphene, metal-MoS_2 and metal-Perovskite LRSPR biosensors. The Perovskite ($CH_3NH_3PbBr_3$) material has unique feature of its outstanding photoelectric, thermal and electrical properties. So, Perovskite materials are widely used in solar cells, photoluminescence converters, microwire lasers, and other fields. Consequently, $CH_3NH_3PbBr_3$ Perovskite has used in the field of optical LRSPR sensors. Wu *et al.* investigated the sensitivity of the LRSPR biosensor with cytop/Al/graphene configuration and found that the sensitivity is enhanced greatly by the introduction of the graphene layer in the LRSPR biosensor configuration [32].

2. Theoretical design and mathematical modeling

The designed structure of the LRSPR biosensor with a thick film of cytop of thickness of 2000 nm is shown in figure 1. The figures 1(a) and (b) are the proposed configurations of Al/MoS_2 and Al/Perovskite based biosensors. All configurations are mounted on the chalcogenide glass (2S2G) prism. Al metal thin film of thickness 15 nm is embedded between cytop and graphene or MoS_2 or Perovskite material. The various configurations of biosensors, cytop/Al/graphene, cytop/Al/MoS_2 and cytop/Al/Perovskite, are considered with biomolecular recognition component as shown in the figure 1. Here, the 2S2G glass with the high refractive index of has been used as the coupling prism. The employed excitation light wavelength (λ) for the LRSPR sensing is 633nm. Especially, the thickness of graphene is taken (d) i.e. d = N x 0.34 nm, where N means number of monolayer of graphene films. In our study, the thicknesses of MoS_2 and perovskite are taken the same as the thickness of the graphene. The TM-polarized electromagnetic (EM) wave is incident on one adjacent side of the 2S2G glass prism and after excitation of the EM wave with the considered configurations; the resultant reflective EM wave is detected on the same side through a photodetector i.e. ATR method Kretschmann configuration [32].

The refractive index (n_1) of the 2S2G prism is taken as [33];

$$n_1 = 2.24047 + \frac{2.693 \times 10^{-2}}{\lambda^2} + \frac{8.08 \times 10^{-3}}{\lambda^4} \tag{1}$$

where λ is understand for wavelength of incident EM wave in micrometers. Subsequent, the sensing medium of $n_s = 1.33$ at $\lambda = 633$ nm is considered due to the very small difference between RI of cytop thin-layer ($n_c = 1.34$), and such periodic arrangement leads to excite LRSPPs in the metallic interface. Furthermore, the dielectric constant of the Al metal layer is, according to the Drude–Lorentz model, given as [34];

$$\varepsilon_m = 1 - \frac{\lambda^2 \lambda_c}{\lambda_p^2(\lambda_c + i\lambda)} \tag{2}$$

where λ_p and λ_c denote the wavelengths of plasma and collision respectively. The values of λ_p and λ_c for aluminum (Al) are 1.0657×10^{-7}m and 2.4511×10^{-5}m respectively. The RI of graphene in observable range is specified by the formula [35] that is given as;

$$n_g = 3.0 + iC_1\frac{\lambda}{3} \tag{3}$$

where $C_1 \approx 5.446\ \mathrm{um}^{-1}$, while λ is the vacuum wavelength in micrometers.

The reflectance of the incident TM-polarized light is calculated by the application of the Transfer Matrix Method [36]. In the proposed structure, entire layers are aligned in the z-direction and each separate layer is well-defined by their d_k thinness, n_k refractive index (RI) and ε_k dielectric constant, where k = 1,2,3. The tangential EM fields at the initial boundary are fixed as $Z = Z_1 = 0$; and the relation of tangential EM fields between initial and final boundary $Z = Z_{n-1}$ is followed as [37];

$$\frac{U_1}{V_1} = M\frac{U_{n-1}}{V_{n-1}} \tag{4}$$

where V_1 and U_1 are magnetic and electric fields at the boundary of the initial layer, V_{n-1} and U_{n-1} are magnetic and electric at the boundary of nth layer, respectively, also M is the total product of all transfer matrices of the collective n layers in the device construction. The TMM is used for TM-polarization light and the total matrix M for considered configuration is specified as [38, 39];

$$M = \prod_{k=2}^{N-1} M_k = \begin{bmatrix} M_{11} & M_{12} \\ M_{21} & M_{22} \end{bmatrix} \tag{5}$$

with

$$M_k = \begin{bmatrix} \cos\beta_k & \dfrac{-i\sin\beta_k}{q_k} \\ -iq_k\sin\beta_k & \cos\beta_k \end{bmatrix} \tag{6}$$

where $q_k = \dfrac{(\varepsilon_k - n_1^2\sin^2\theta_1)^{1/2}}{\varepsilon_k}$ and $\beta_k = \dfrac{2\pi d_k(\varepsilon_k - n_1^2\sin^2\theta_1)^{1/2}}{\lambda}$, Here, θ_1 is the angle of incidence of electromagnetic wave on the base of 2S2G glass prism. Using TMM, and we can obtain four elements of electric and magnetic fields in the characteristics matrix M for periodic layers; M_{11} M_{12} M_{21} and M_{22}. By application of these essentials components, we can compute the coefficient of total reflection r_p for TM or p-polarization light and the relation is given as follows [40];

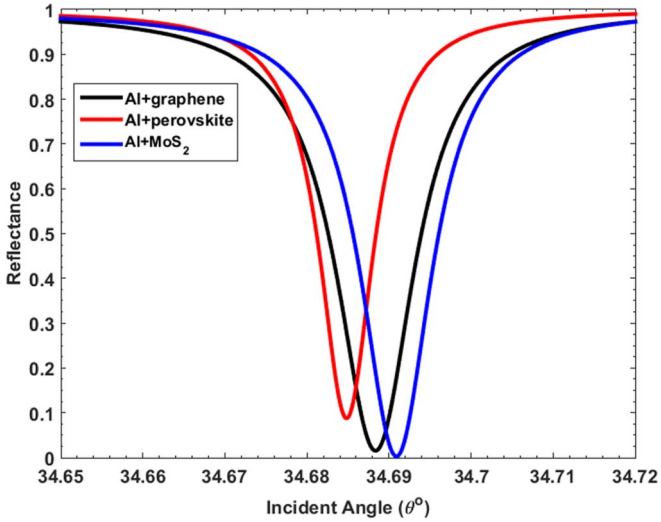

Figure 2. Reflectance of the designed biosensors as a function of incident angle for the configurations of Al/different materials.

$$r_p = \frac{(M_{11} + M_{12}q_n)q_1 - (M_{21} + M_{22}q_n)}{(M_{11} + M_{12}q_n)q_1 + (M_{21} + M_{22}q_n)} \tag{7}$$

Lastly, the reflectance R_p of n layers for p-polarization is calculated by;

$$R_p = |r_p|^2 \tag{8}$$

The variation in the n_s RI of the sensing medium can lead to alteration in reflectance R and the maximum change in R can yield a maximum sensitivity (S). Therefore, the sensitivity (S) can be defined as follows;

$$S = \frac{dR_p}{dn_s}, \tag{9}$$

Now, for the proposed SPR sensor we can obtain the detection accuracy (DA) from the resulting reflective curves using full width at half maximum (FWHM) from the reflectance of the layered materials. [41];

$$DA = \frac{1}{FWHM} \tag{10}$$

To get the maximum performance sensor, the DA must be maximum as possible. It is apparent that the detection accuracy is inversely proportion to FWHM, consequently, a finer FWHM will produce a maximum DA.

3. Results and discussion

In this work, we have proposed LRSPR biosensor consisting different configurations with aluminum metal layer and the sensitivity of the considered LRSPR biosensors was studied and the sensitivities are compared with the conventional metal-graphene LRSPR biosensor. If the materials loss is low, then the sensitivity of the LRSPR sensors is enhanced because the propagation distance and penetration depth of surface plasmon polaritons are longer and deeper than other metals. Besides this, Al is the low-cost material as well as minimum internal damping than the other plasmonic materials [34, 42]. Al better-satisfied surface plasmon resonance (SPR) condition in the Kretschmann configuration, the sensitivity and detection accuracy of such configurations are better than the silver and other plasmonic materials. Now the proposed LRSPR biosensors based on Al/graphene or Al/MoS_2 or Al/Perovskite layers can be used for biomolecular recognition element. For our calculation convenience, we have taken the complex refractive index of MoS_2 and $CH_3NH_3PbBr_3$ Perovskite is $5.2227 + 1.0804i$ and $2 + 0.003i$ at $\lambda = 633$ nm respectively [43–47]. The fluorine-containing insulating polymer, poly perfluorobutenylvinylether, called Cytop, is used as a small RI layer in the LRSPR sensor [48]. The Cytop is an amorphous material and transparent fluoropolymer through maximum solubility and the film-forming virtues of cytop at room temperature is also frequently considered as the insulating film in field-effect transistors [49]. Furthermore, the RI of cytop is $n_1 = 1.34$ at $\lambda = 633$ nm, which is extensively used as matching film in SPR sensor [50].

The reflectance (R), sensitivity (S), detection accuracy (DA) and other properties of designed structure at different parameters are studied in four subsections. In the first subsection, we study the reflectance and

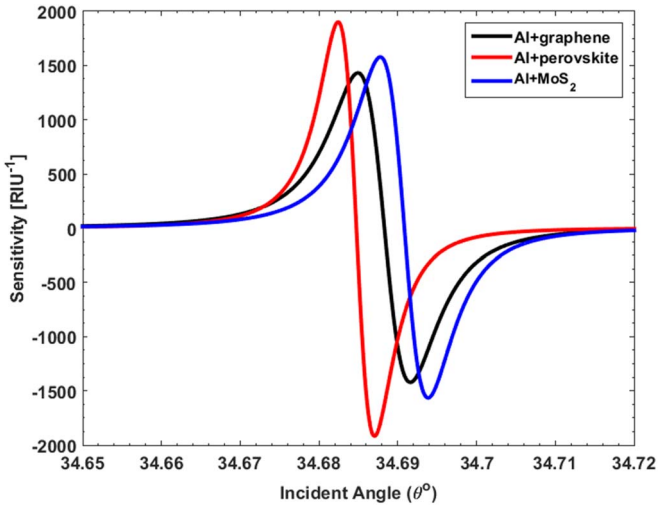

Figure 3. Sensitivity of the designed biosensors as a function of incident angle for the configurations of Al-different materials.

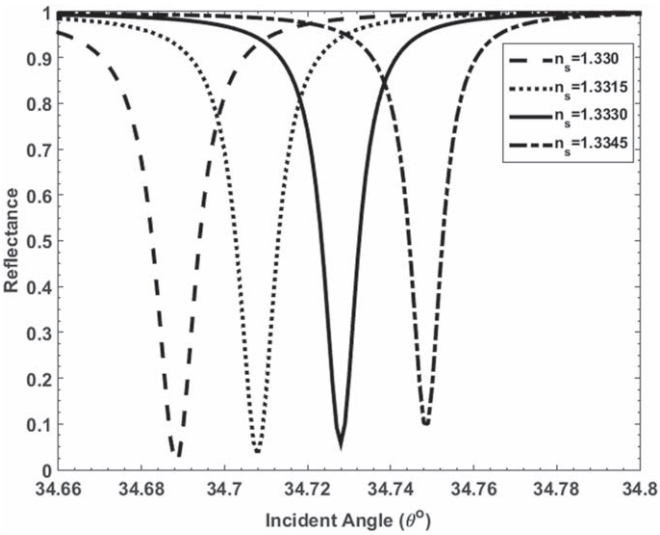

Figure 4. Reflectance of the designed Al-graphene biosensor as a function of incident angle by variation of n_s.

sensitivity properties by using the TMM for TM mode. In the second subsection, we study the variation of reflectance with the variation of RI of sensing medium. In the third subsection, we study the sensitivity variation by variation of layer or width of layer. We study the FWHM and DA of the considered configurations in the last subsection.

3.1. Reflectance and sensitivity of different configurations of considered biosensor

The reflectance and sensitivity of designed structure are calculated by using TMM method for EM wave with wavelength 633 nm and RI of sensing medium $n_s = 1.33$. Figure 2 shows the variation of reflectance versus incident angle for different biosensor configurations. The reflectance of Al based sensors for all combinations (Al-graphene or Al-MoS_2 or Al-Perovskite) are compared. The black curve shows the variation of reflectance regarding incident angle for combination of Aluminum-graphene layer as a conventional LRSPR optical biosensor. The red curve and blue curves show the variation of reflectance versus incident angle for corresponding Al-Perovskite layer and Al-MoS_2 layer configurations respectively. In comparison of the all reflectance, the reflectance for Al-MoS_2 is found zero at the 34.692° resonance angle and this is most fruitful and suitable configuration for high efficiency and high accuracy LRSPR biosensor.

In figure 3, the sensitivity versus incident angle has been shown, the black, red and the blue curves represent the sensitivity of Al-graphene, Al-Perovskite and Al-MoS_2 layers, respectively. Depending on the surroundings and angle of incidence the peak sensitivity for the configuration of Al-graphene layer is found to be 1430 RIU^{-1} at 34.69° resonance angle. Similarly, peak sensitivity for the configuration of Al-Perovskite and Al-MoS_2 layers

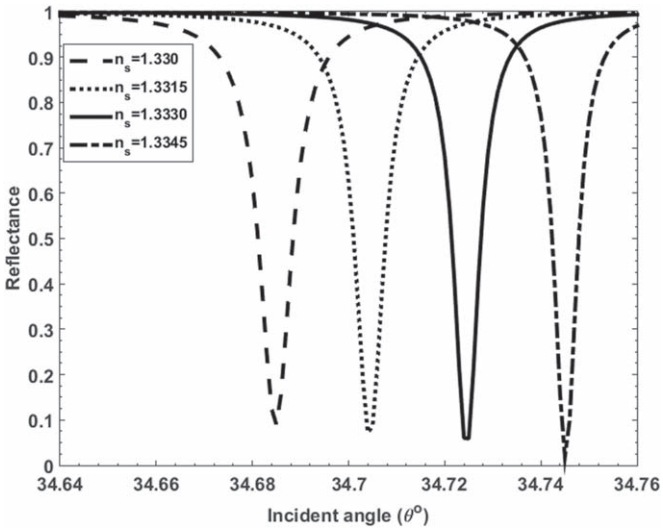

Figure 5. Reflectance of the designed Al-Perovskite biosensor as a function of incident angle by variation of n_s.

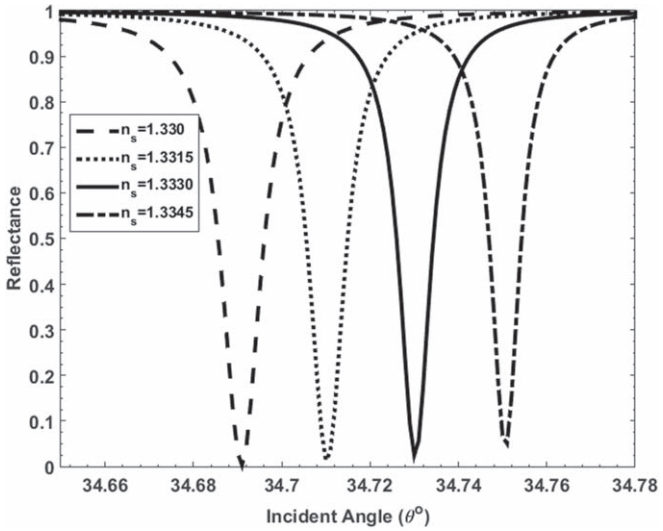

Figure 6. Reflectance of the designed Al-MoS_2 biosensor as a function of incident angle by variation of n_s.

are found to be 1857.6 RIU^{-1} at 34.68° resonance angle and 1571.6 RIU^{-1} at 34.69° resonance angle respectively. From the above results, it is evident that the proposed LRSPR biosensors with the configuration of Al metal layer and Perovskite layer combination have higher peak sensitivity in comparison to the others LRSPR biosensor configurations.

3.2. Reflectance with the variation of RI of sensing medium (n_s)

The reflectance at 633 nm wavelength is studied with the variation of n_s for all configurations. Now, figures 4–6 show the reflectance versus resonance angle for the configurations of Al-graphene, Al-Perovskite, and Al-MoS_2 layers respectively with the variation of refrective indices of sensing medium n_s range from 1.3300 to 1.3345.

3.3. Peak sensitivity variation with layers or thicknesses and refractive indices

The peak sensitivity of the considered LRSPR biosensors is varied with number of layers and thicknesses of the sensing material. The peak sensitivity is an important factor to influence the performance of the proposed biosensor. The figure 7 demonstrates the variation of maximum sensitivity with respect to the number of layers for the proposed LRSPR biosensor based on Al-graphene, Al-MoS_2 and Al-perovskite for 633 nm source wavelength and 1.33 sensing medium RI. The thickness of the graphene, MoS_2 and perovskite layer is taken as $N \times 0.34$ nm, where N is number of layers. For Al-graphene layer configuration, the black line shows the variation of peak sensitivity by increasing the number of graphene layers. The maximum peak sensitivity for Al-

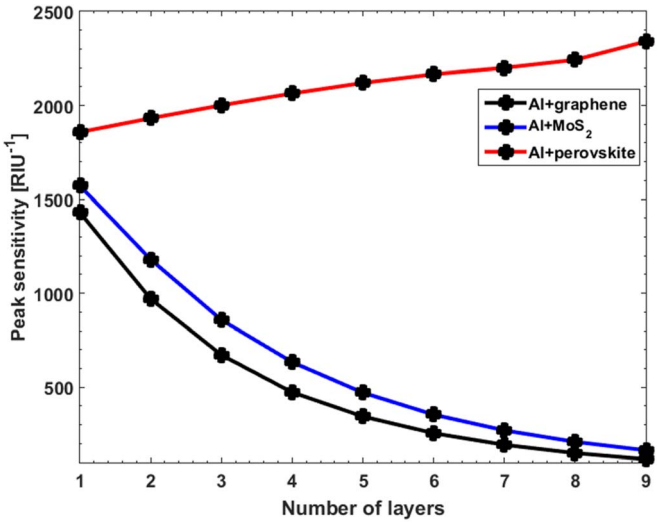

Figure 7. Peak sensitivity of designed structure at different number of layers (N) where the thickness of materials for all configurations is Nx0.34 nm.

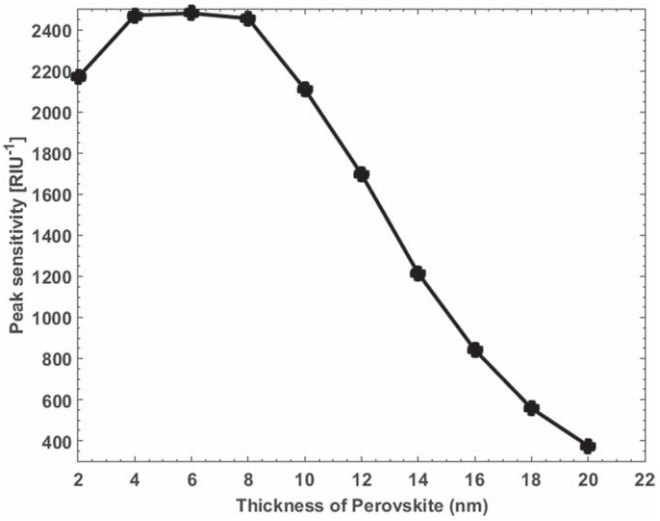

Figure 8. Peak sensitivity of designed structure at different thicknesses (nm) of the perovskite.

graphene configuration with single layer of graphene is to be found 1430 RIU^{-1}. Similarly, the blue line shows the peak sensitivity of the Al-MoS_2 configuration for variation of MoS_2 layers and the red line shows the peak sensitivity of Al-Perovskite, which is increased with increase the thickness of the MoS_2 and Perovskite i.e. increase number of graphene layers. The thickness of MoS_2 and Perovskite is equal to the multiple of 0.34nm to number of layer. The maximum peak sensitivity of the biosensor is found 1571 RIU^{-1} for single layer MoS_2 layer. This result reveals that the single layer of the graphene and MoS_2 shows maximum sensitivity, but the synthesis of the single layer of graphene or MoS_2 layer is very complicated. Therefore, we would look into another material like Perovskite that is used in many devices. So, Perovskite materials can be used for simple synthesis for LRSPR biosensor and sensitivity may be high due to its easily transport of charge carriers. In the study, reflectance and peak sensitivity of the configuration of Al-Perovskite layer has found to be 1857.6 RIU^{-1} at 34.68° for the thickness 0.34 nm, which better than another configuration. So, we have emphasized on the LRSPR biosensor based on the Perovskite layer as sensing material and studied the peak sensitivity by variation of width of Perovskite layer.

The peak sensitivity of Al-Perovskite configuration is increased with increase of the thickness of the Perovskite layer. Figure 8 shows the variation of peak sensitivity by variation of thickness of perovskite layer for Al-Perovskite configuration LRSPR biosensor. The peak sensitivity of Al-Perovskite is increased firstly with increases thickness of Perovskite layer upto 8 nm and then it is started to decrease with increases thickness of

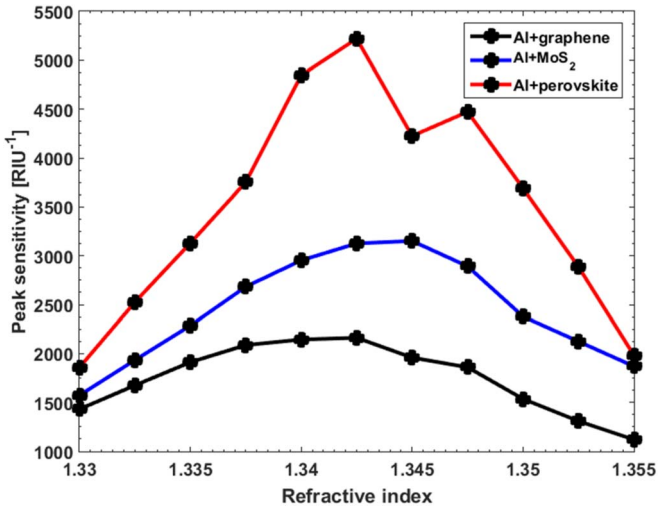

Figure 9. Peak sensitivity versus refractive index of sensing medium for all configurations.

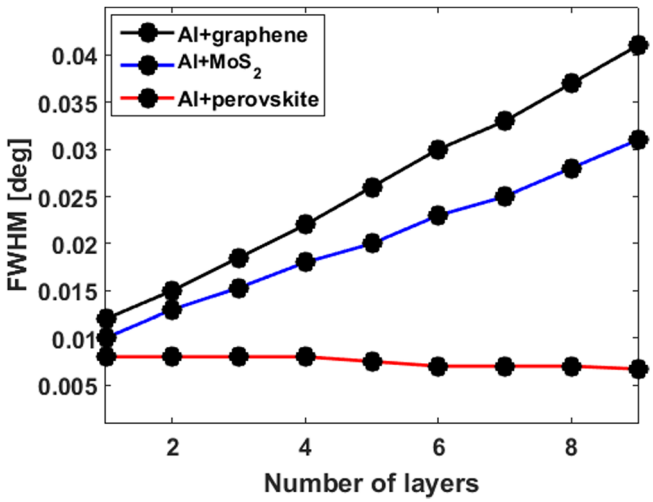

Figure 10. Variation of FWHM with number of layers at different configuration of periodic layers.

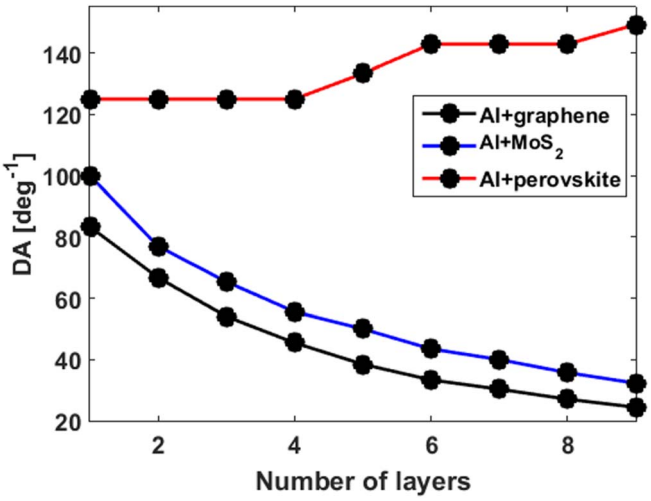

Figure 11. Detection accuracy (DA) versus layers.

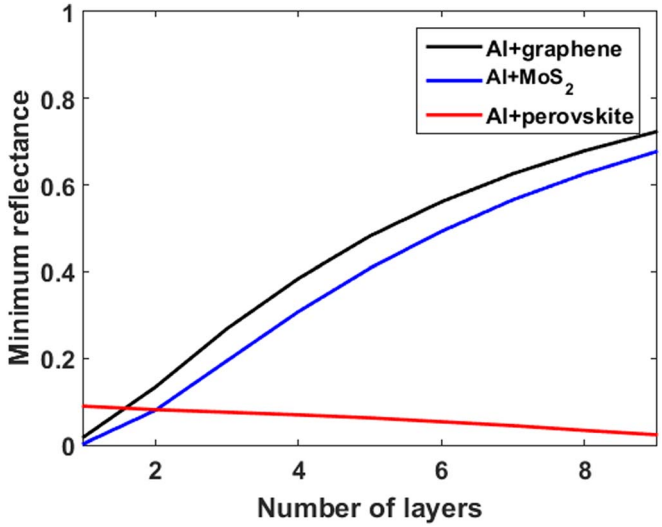

Figure 12. Minimum reflectance versus thickness of materials (~L × 0.34 nm), where L is number of layers.

Table 1. Comparative table for sensitivity of the biosensor with different configurations.

Configuration	Sensitivity	Reference
Al + perovskite	1857.6 RIU^{-1}	Our result
Al + MoS_2	1571.6 RIU^{-1}	Our result
Al + graphene	1430.0 RIU^{-1}	[41]
Graphene/Ag-based SPR sensor	455.4 RIU^{-1}	[51]
TMDCs/Al-based SPR sensor	895.6 RIU^{-1}	[52]
TMDCs/Au-based LRSPR biosensor	1240.2 RIU^{-1}	[53]

Perovskite layer above 8 nm. The maximum peak sensitivity is found to be 2482 RIU^{-1} for 6.5 nm thickness of Perovskite layer at $\lambda = 633$ nm and $n_s = 1.33$.

Figure 9 shows the variation of peak sensitivity versus RI of sensing medium n_s. The black curve, the blue curve and the red curve are the variation of peak sensitivity of Aluminum- graphene, Aluminium-MoS_2 and Aluminium-Perovskite, respectively with thickness of Aluminium is fixed i.e. 15 nm and thicknesses of other materials are taken equivalent to single layer graphene i.e. 0.34 nm. Here, it is inferred that the peak sensitivity for graphene, MoS_2 and Perovskite layer is increased by n_s; but the sensitivity of Perovskite layer, in comparison to both materials, is increased sharply by increasing n_s and found to be the maximum value 5220 RIU^{-1} at 34.87° for $n_s = 1.3425$. After this maximum value of the sensitivity, it starts to decrease. This result reveals that the peak sensitivity of the Al-Perovskite configuration has best for the sensing medium of refractive index around 1.3425.

3.4. Variation of full width half maxima (FWHM) and detection accuracy (DA)

For the LRSPR biosensors, the FWHM (figure 10) and DA (figure 11) are also the important factors to show the performance of the biosensor as increase the thickness of the sensing materials. Due to the high absorbing layers, the dip of the LRSPR reflectance curve get finer and the FWHM becomes wider. However, the DA of the LRSPR is the reciprocal of the FWHM. The studies show that the DA of the Perovskite material is found very high in comparison to the others materials because the FWHM is very low for Perovskite material. Moreover, the resonance angle of LRSPR reflectance curve alters from low to high angles with the increase of layers as shown in the figure 12. A comparative table 1. 1 for sensitivity of the biosensor with different configurations is given and indicates that the sensitivity of proposed Al-MoS_2 and Al-Peroskite based LRSPR biosensors has found nearly 10% and nearly 30% more sensitive than the standard Al-graphene LRSPR biosensor.

4. Conclusion

In this communication, we have proposed a new configuration of LRSPR biosensors based on the Al-MoS_2 and Al-Perovskite. The proposed confugations have found the enahanced sensitivity and high detection accuracy in

comparison to conventional Al-graphene LRSPR biosensor. However, the sensitivity of proposed LRSPR biosensor based on the Al-Perovskite with thickness of Perovskite material 0.34 nm has highest peak sensitivity (4847 RIU^{-1}) for sensing medium of RI 1.34, which is highest value for the LRSPR biosensors. Moreover, the sensitivity of proposed Al-MoS_2 based LRSPR biosensor is nearly 10% more sensitive than the standard Al-graphene LRSPR biosensor, while Al-Peroskite based with same congiuration type have nearly 30% more sensitive than the standard Al-graphene LRSPR biosensor.

Acknowledment

One of the authors, Mr Mohit Kumar, acknowleges Babasaheb Bhimrao Ambedkar University Lucknow for providing non-NET fellowship.

Data availability statement

All data that support the findings of this study are included within the article (and any supplementary files).

ORCID iDs

Khem B. Thapa https://orcid.org/0000-0003-2639-0652

References

[1] Fink Y, Winn J N, Fan S, Chen C, Michel J, Joannopoulos J D and Thomas E L 1998 A dielectric omnidirectional reflector *Science* **282** 1679–82
[2] Wu F, Lyu K, Hu S, Yao M and Xiao S 2021 Ultra-large omnidirectional photonic band gaps in one-dimensional ternary photonic crystals composed of plasma, dielectric and hyperbolic metamaterial *Opt. Mater.* **111** 110680
[3] Wu F, Wu X, Xiao S, Liu G and Li H 2021 Broadband wide-angle multilayer absorber based on a broadband omnidirectional optical tamm state *Opt. Exp.* **29** 23976–87
[4] Yablonovitch E 1987 Inhibited spontaneous emission in solid-state physics and electronics *Phys. Rev. Lett.* **58** 2059–62
[5] Joannopoulos J D, Villeneuve P R and Fan S 1997 Photonic crystals: putting a new twist on light *Nature* **386** 143–9
[6] Joannopoulos J D, Johnson S G, Winn J N and Meade R D 2008 *Photonic Crystals: Molding Flow of Light* (New Jersey: Princeton University Press)
[7] Inan H, Poyraz M, Inci F, Lifson M A, Baday M, Cunningham B T and Demirci U 2017 Photonic crystals: emerging biosensors and their promise for point-of-care applications *Chem. Soc. Rev.* **46** 366–88
[8] Fenzl C, Hirsch T and Wolfbeis O S 2014 Photonic crystals for chemical sensing and biosensing *Angew. Chem. Int. Ed. Engl.* **53** 3318–35
[9] Chen H, Lou R, Chen Y, Chen L, Lu J and Dong Q 2017 Photonic crystal materials and their application in biomedicine *Drug Deliv.* **24** 775–80
[10] Rajasekar R and Robinson S 2019 Photonic crystal-based sensors for biosensing applications *Book: Advances in Photonic Crystals and Devices* ed N Kumar and B Suther (United States: CRC Press, Taylor Francis)
[11] El-Amassi D M, Taya S A and Vigneswaran D 2018 Temperature sensor utilizing a ternary photonic crystal with a polymer layer sandwiched between Si and SiO_2 layers *J. Theor. Appl. Phys.* **12** 293–8
[12] Singh B K and Pandey P C 2016 Effect of temperature on terahertz photonic and omnidirectional band gaps in one-dimensional quasi-periodic photonic crystals composed of semiconductor InSb *Appl. Opt.* **55** 5684–92
[13] Lu T-W, Wu C-C and Lee P-T 2018 1D photonic crystal strain sensors *ACS Photonics* **5** 2767–72
[14] Ramanujam N R, Amiri I S, Taya S A, Olyaee S, Udaiyakumar R, Pandian A P, Wilson K S J, Mahalakshmi P and Yupapin P P 2019 Enhanced sensitivity of cancer cell using one dimensional nano composite material coated photonic crystal *Microsystem. Technol.* **25** 189–96
[15] Maier S A 2007 *Plasmonics: Fundamentals and Applications* (Berlin: Springer) ISBN: 978-0-387-33150-8.
[16] Emami Nejad H, Mi A and Farmani A 2019 Supersensitive and tunable nano biosensor for Cancer detection *IEEE Sens. J.* **19** 4874–81
[17] El-Khozondar H J, Mahalakshmi P, El-Khozondar R J, Ramanujam N R, Amiri I S and Yupapin P 2019 Design of one dimensional refractive index sensor using ternary photonic crystal waveguide for plasma blood samples applications *Physica E: Low-dim. Syst. Nanostr.* **111** 29–36
[18] Raether H 1988 *Surface Plasmons on Smooth and Rough Surfaces and on Gratings.* (Berlin, Germany: Springer)
[19] Hutter E and Fendler J H 2004 Exploitation of localized surface plasmon resonance *Adv. Maters.* **16** 1685–706
[20] Hickel W, Kamp D and Knoll W 1989 Surface-plasmon microscopy *Nature* **339** 186
[21] Gao Y, Xin Z, Zeng B, Gan O, Cheng X and Bartoli F J 2013 Plasmonic interferometric sensor arrays for high-performance label-free biomolecular detection *Lab Chip* **13** 4755–64
[22] Barik A, Otto L M, Yoo D, Jose J, Johnson T W and Oh S-H 2014 Dielectrophoresis-Enhanced Plasmonic Sensing with Gold Nanohole Arrays *Nano Lett.* **14** 2006–12
[23] Zeng B, Gao Y and Bartoli F J 2014 Rapid and highly sensitive detection using Fano resonances in ultrathin plasmonic nanogratings *Appl. Phys. Lett.* **105** 161106
[24] Zeng B, Gao Y and Bartoli F J 2015 Differentiating surface and bulk interactions in nanoplasmonic interferometric sensor arrays *Nanoscale* **7** 166–70
[25] Dai X, Jiang L and Xiang Y 2015 Low threshold optical bistability at terahertz frequencies with graphene surface plasmons *Sci Rep.* **5** 12271

[26] Dai X, Jiang L and Xiang Y 2015 Tunable THz Angular/Frequency filters in the modified kretschmann–raether configuration with the insertion of single layer *Graphene, IEEE Photon. J.* **7** 5500808
[27] Johansen K, Arwin H, Lundström I and Liedberg B 2000 Imaging surface plasmon resonance sensor based on multiple wavelengths: sensitivity considerations *Rev. Sci. Instrum.* **71** 3530–8
[28] Sarid D 1981 Long-range surface-plasma waves on very thin metal films *Phys. Rev. Lett.* **47** 1927–30
[29] Matsubara K, Kawata S and Minami S 1990 Multilayer system for a high-precision surface plasmon resonance sensor *Opt. Lett.* **15** 75–7
[30] Krupin O, Asiri H, Wang C, Tait. R N and Berini P 2013 Biosensing using straight long-range surface plasmon waveguides *Opt. Exp.* **21** 698–709
[31] Love J C, Estroff L A, Kriebel J K, Nuzzo R G and Whitesides G M 2005 Self-assembled monolayers of thiolates on metals as a form of nanotechnology *Chem. Rev.* **105** 1103–69
[32] Wu L, Ling Z, Jiang L, Guo J, Dai X, Xiang Y and Fan D 2016 Long-range surface plasmon with graphene for enhancing the sensitivity and detection accuracy of biosensor *IEEE Photonics J.* **8** 4801409
[33] Maharana P K and Jha R 2012 Chalcogenide prism and graphene multilayer based surface plasmon resonance affinity biosensor for high performance *Sensors and Actuators: B. Chem.* **169** 161–6
[34] Sharma A K and Gupta B D 2007 On the performance of different bimetallic combinations in surface plasmon resonance based fiber optic sensors *J. Appl. Phys.* **101** 093111
[35] Bruna M and Borini S 2009 Optical constants of graphene layers in the visible range *Appl. Phys. Lett.* **94** 031901
[36] Yamamoto M 2002 Surface plasmon resonance (SPR) theory: tutorial *Encyclopedic Reference of Immunotoxicology* **14** 388–98
[37] Zeng S, Hu S, Xia J, Anderson T, Dinh X-Q, Meng X-M, Coquet P and Yong K-T 2015 Graphene-MoS_2 hybrid nanostructures enhanced surface plasmon resonance biosensors *Sensors and Actuators: B. Chem.* **207** 801–10
[38] Maharana P K, Jha R and Palei S 2014 Sensitivity enhancement by air mediated graphene multilayer-based surface plasmon resonance biosensor for near infrared *Sensors and Actuators: B. Chem.* **190** 494–501
[39] Verma R, Gupta B D and Jha R 2011 Sensitivity enhancement of a surface plasmon resonance-based biomolecules sensor using graphene and silicon layers *Sensors and Actuators: B. Chem.* **160** 623–31
[40] Wu L, Chu H S, Koh W S and Li E P 2010 Highly sensitive graphene biosensors based on surface plasmon resonance *Opt. Express* **18** 14395–400
[41] Maharana P K, Srivastava T and Jha R 2014 On the performance of highly sensitive and accurate graphene-on-aluminum and silicon-based SPR biosensor for visible and near infrared *Plasmonics* **9** 1113–20
[42] Wang Q, Jinga J-Y and Cheng Z 2021 Long-range surface plasmon resonance and its biological sensing applications, chapter-Eight, Handbook on Comprehensive *Anal. Chem.* **95** 277–338
[43] Maurya J B, Francois A and Prajapati Y K 2018 Two-dimensional layered nanomaterial-based one dimensional photonic crystal refractive index sensor *Sensors* **18** 857
[44] Beal A R and Hughes H P 1979 Kramers-Kronig analysis of the reflectivity spectra of 2H-MoS2, 2H-MoSe2 and 2H-MoTe2 *J. Phys. C: Solid State Phys.* **12** 881 (https://refractiveindex.info/?shelf=main&book=MoS2&page=Beal)
[45] Beal A R and Hughes H P 1979 Kramers-kronig analysis of the reflectivity spectra of 2H- MoS_2, 2H-$MoSe_2$ and 2H-$MoTe_2$ *J. Phys. C: Solid State Phys.* **12** 881–90
[46] Brittman S and Garnett E C 2016 Measuring n and k at the microscale in single crystals of $CH_3NH_3PbBr_3$ perovskite *J. Phys. Chem. C* **120** 616–20
[47] Zhang H, Ma Y, Wan Y, Rong X, Xie Z, Wang W and Dai L 2015 Measuring the refractive index of highly crystalline monolayer MoS_2 with high confidence *Sci Rep.* **5** 8440
[48] Zheng Y, Shi W, Kong J, Huang D, Katz H E, Yu J, Taylor A D and Cytop A 2017 *Insulating Tunneling Layer for Efficient Perovskite Solar Cells, Small Methods* **1** 1700244
[49] Huang W *et al* 2014 Label-free brain injury biomarker detection based on highly sensitive large area organic thin film transistor with hybrid coupling layer *Chem. Sci.* **5** 416–26
[50] Yue C, Lang Y, Zhou X and Liu Q 2019 Sensitivity enhancement of an SPR biosensor with a graphene and blue phosphorene/transition metal dichalcogenides hybrid nanostructure *Appl. Opt.* **58** 9411–20
[51] Maharana P K, Jha R and Padhy P 2015 On the electric field enhancement and performance of SPR gas sensor based on graphene for visible and near infrared *Sensors and Actuators: B. Chem.* **207** 117–22
[52] Xu Y, Wu L and Ang L K 2019 MoS_2 Based highly sensitive near-infrared surface plasmon resonance refractive index sensor *IEEE J. Selected Topics Quant. Electronics* **25** 1–7
[53] Xu Y, Hsieh C-Y, Wu L and Ang L K 2019 Two dimensional transition metal dichalcogenides mediated long range surface plasmon resonance biosensors *J. Phys. D* **52** 065101